CHAPTER 4. Oxidation of the arsenic-rich concentrate at the Přebuz abandoned mine (Erzgebirge Mts., CZ): the mineralogical evolution

Filippi[a] M.

[a] Institute of Geology, v.v.i., Academy of Sciences of the Czech Republic, Rozvojová 269, 165 02 Prague 2, Czech Republic

Status: Published in journal the Total Science of the Environment, 322, (2004): 271-282

Abstract

Ore concentrate with up to 65 wt.% of arsenic (by-product of cassiterite extraction) exposed to climatic conditions was studied from the mineralogical point of view. Detailed sampling, X-ray diffraction analyses (XRD), energy-dispersive microanalysis (EDAX) and especially scanning electron microscopy (SEM) were applied to study the arsenopyrite-löllingite- concentrate weathering. The studied concentrate contains very small proportion (<5 vol.%) of gangue minerals such as quartz and feldspars; the oxidation of arsenopyrite and löllingite (and accessory pyrite) is thus practically not complicated by interference with additional minerals and elements. Arsenolite, scorodite, kaatialaite and native sulphur were found to be the main secondary phases originating by dissolution of arsenopyrite and löllingite. New secondary phases precipitate on the surface of the ore-concentrate body but also form cement among the grains of finely milled material. The following succession of secondary minerals was determined: arsenolite, scorodite + native sulphur and kaatialaite. Significant arsenic migration into the proximal environment was revealed: 2580 and 13,622 mg kg^{-1} were the highest arsenic concentrations in two sections excavated at distances of 0.5 and 1.5 m from the concentrate body.

Keywords: arsenic concentrate, oxidation, arsenopyrite, löllingite, arsenic secondary minerals

4.1. Introduction

Arsenopyrite (FeAsS) is a significant mineral in many types of ore associations (Ramdor, 1980) and hence the most common arsenic (As) mineral in nature (Vink, 1996). Nevertheless, it is of limited economic importance and is generally discarded during mining processes (Nesbitt et al., 1995). Löllingite (FeAs2) belongs among moderately common As minerals but its oxidation has not been widely studied. Under exposure to climatic effects both minerals are unstable and their oxidation leads to As release and contamination of the environment. Therefore, chiefly arsenopyrite has been studied by many authors. Several experimental works were aimed at arsenopyrite oxidation (e.g., Buckley and Walker, 1988; Richardson and Vaughan, 1989; Nesbitt et al., 1995; Nesbitt and Muir, 1998). Other experiments were focused on precipitation and stability of scorodite (FeAsO4 · 2H2O) as the most common product of arsenopyrite oxidation (e.g., Dove and Rimstidt, 1985; Nordstrom and Parks, 1987; Krause and Ettel, 1988).

A number of real cases were studied in field also recently to understand As behaviour in different types of environments, mostly in contaminated water sediments, soils and in numerous types of mine waste and tailings (e.g., Bowell, 1994; Voigt et al., 1996; Craw et al., 1999; Hudson-Edwards et al., 1999; Langmuir et al., 1999; Juillot et al., 1999; Corwin et al., 1999; Donahue et al., 2000; Savage et al., 2000; Nickson et al., 2000; Lumsdon et al., 2001; Pichler et al., 2001; Williams, 2001; Anawar et al., 2002). However, many pitfalls may be associated with the generalization of results.

From the mineralogical point of view, the secondary phases originating during oxidation of ore minerals are often insufficiently identified, which reduces the possibility of comparison between experimental data and field observations. This can be explained mostly by the scarcity of the studied phase (common occurrence as thin coatings on dispersed relicts of ore grains, intimate intergrowth of several minerals, and also by the high complexity of these species and consequently their poor knowledge). As a result, only general identifications of these secondary phases can be often found in the literature: e.g., scorodite-like minerals and Fe-As-O minerals in Foster et al. (1998) and Hudson-Edwards et al. (1999), respectively, Ca- (Ca-Fe-), etc., arsenates in Alpers et al., (1994); Sidenko et al., (1998); Lazareva and Pospelova, (1998); Donahue et al., (2000), Fe-rich arsenates (e.g., Pichler et al., 2001). The understanding of processes in every other case of As-ore oxidation followed by secondary minerals precipitation, therefore, extends our knowledge of As behaviour in the environment. Only complex information (field characteristics as well as experimental modelling) can lead to complex solution of specific cases (as in Juillot et al., 1999; Langmuir et al., 1999).

In this respect, the case presented below offers a good opportunity to study weathering of two arsenic minerals under very specific conditions with evident oxidation products.

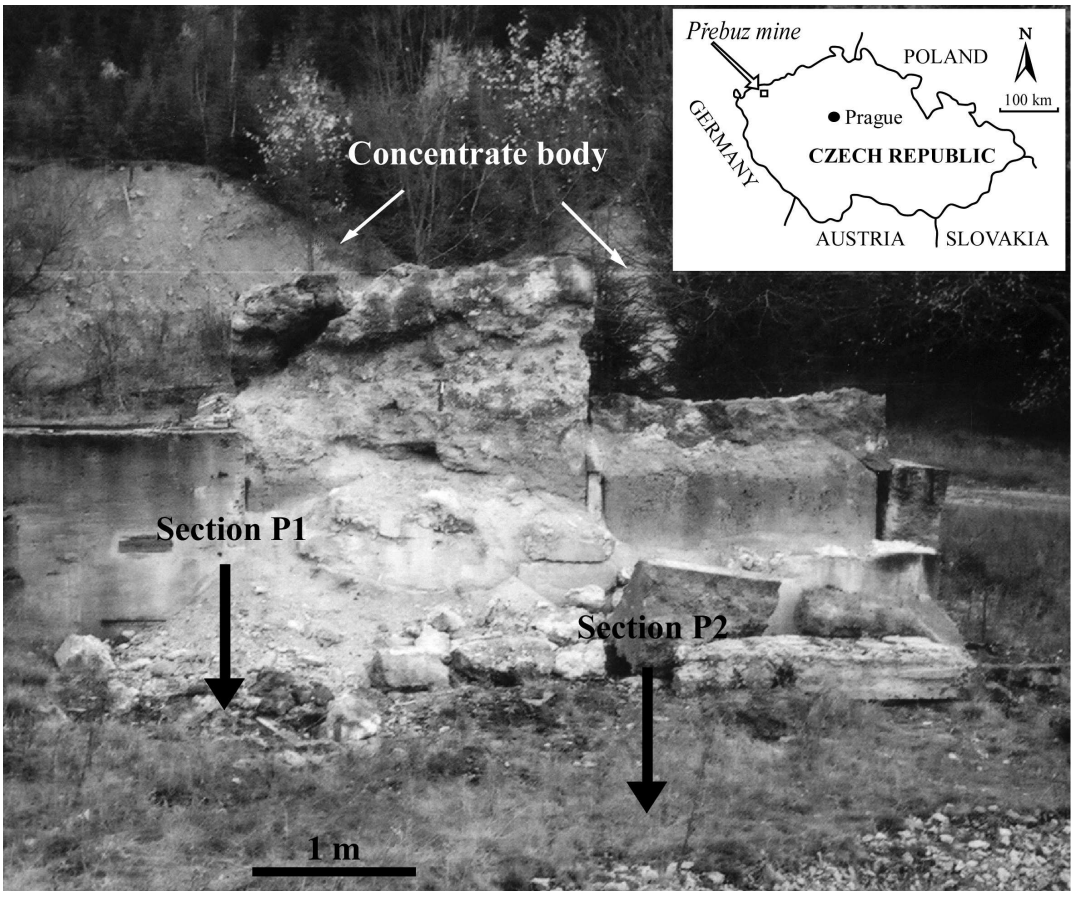

Fig. 1. Location map of the abandoned Přebuz mine and settings in the close proximity of the concentrate body (position of sections P1 and P2 are marked by arrows).

4.2. Geological setting and description of the concentrate

The abandoned tin mine near Přebuz is located in the northern part of the Bohemian Massif in area of the Krušné hory Mts. (Fig. 1). Place mining followed by underground mining for cassiterite (SnO_2) in this area commenced in the 13th century but the main exploitation of this deposit dates to the periods of 1938–1945 and 1950–1957 (Rojík, 2000). Tin mineralisation is bound to greisenized zones in granite (Kratochvíl, 1954; Škvor, 1960). Zoubek (1951) ranked these autometamorphosed granites within the Erzgebirge type belonging to the Nejdek massif. The principal ore minerals were cassiterite, arsenopyrite, löllingite, hematite (Fe_2O_3), and rarely also wolframite [$(Fe,Mn)WO_4$]. Other minerals present in the mineralized zones were apatite, autunite, fluorite, opal, pyrite, topaz, and torbernite (Bernard, 1981). However, absolutely prevailing ore minerals were arsenopyrite and löllingite (Hak, 1960). Upon mining (1940–1945) the exploited ore was processed directly in the area of the plant, using the method of gravitational flotation (Kratochvíl, 1954). The obtained concentrates (tin and arsenic concentrates) were exported to Germany for additional processing, but a part of the arsenic concentrate (with up to 65 wt.% arsenic, Kratochvíl, 1954) was stored in the area of the dressing plant. The first short report about the existence of the Přebuz arsenic anomaly was given by Šrein et al. (1999).

Finely milled arsenic concentrate was enclosed in a concrete bunker (c. 5x3x2 m in size), which practically prevented any possible changes of ore minerals. After some time, the bunker was partly destroyed (ceiling and frontal panels were removed) and the concentrate was exposed to climatic effects (Fig. 1). According to the available information (P. Rojík and V. Machovič – oral communication) the destruction of the bunker was documented some time before 1983. The exposure of the concentrate started changes of primary minerals on a large scale. At present, the concentrate body is strongly consolidated and covered by secondary minerals.

4.3. Methods and sample description

Detailed sampling and documentation of the concentrate body was undertaken. Not only surface but also subsurface samples (down to the depth of c. 20 cm) and highly weathered concentrate fragments near the bunker were collected. More than 30 samples were acquired and studied under a binocular microscope. Eight apparently different secondary phases, based on their colour and morphology, were selected for powder diffraction analyses. Also one mixed sample with all distinguishable assumed mineral species was prepared as a verification of the integrity of separation.

X-ray diffraction analyses (XRD) employed PHILIPS X´PERT diffractograph under these conditions: CuKα radiation, graphite secondary monochromator, 35 kV, 30 mA, step scanning at 0.05^o/3s in the range of 2-60^o 2θ (analyst J. Dobrovolný). The ZDS-system software, version 6.01 (Ondruš, 1995) and the powder diffraction file PDF-2 were used for peak identification.

Chemical composition and micromorphology of mineral phases were studied on JEOL JXA-50, an electron microanalyser with EDAX PV 9400 (EDAX) in Service Laboratory of Physical Methods, Institute of Geology AS CR (analysts A. Langrová and V. Böhmová). Operating conditions were: polished sections coated with carbon (for analyses and backscattered electron image), mineral fragments coated with gold (for micromorphology), voltage 20 kV, probe current 1.4 nA and counting time 60 sec. ZAF correction procedures were used for the calculation. The following standards were used: GaAs (As), hematite (Fe), leucite (K), jadeite (Al, Si), ZnS (sulphidic S) and barite (Ba, sulphate

S). Images using backscattered (BSE) and secondary electrons (SEI) and element distributions were studied by the author on a CamScan S4 (SEM) scanning electron microscope with Link ISIS 300 energy-dispersive spectrometer in the Geological Laboratories, Faculty of Science, Charles University, Prague. The following types of samples were used for SEM and EDAX investigations:

- arsenic concentrate samples macroscopically unaffected by weathering (seemingly composed of ore minerals only),
- slightly weathered arsenic concentrate samples (with apparent thin powdery cover of secondary minerals on the surface),
- highly weathered arsenic concentrate samples (secondary phases prevail over ore particles),
- highly weathered arsenic concentrate samples practically without ore particles.

Polished sections were orientated perpendicular to the weathered core covering the concentrate material to enable the observation of possible zoning incurred by weathering.

Two sections (P1 and P2 – for characteristics see Table 2) were excavated in the anthropogenic soil material (landfill) to evaluate arsenic contamination in the close vicinity of the arsenic concetrate body. Partial bunker disturbance and terrain morphology enabled outflow of solutions just in one direction. Both sections were situated in the affected area (Fig. 1). After drying (at room temperature) the samples (0.5–1 kg) were sieved to 2 mm. Selected samples were prepared for arsenic determination according to the method A of Van der Veen et al. (1985). 1 g of sample and 7.5 ml of concentrated nitric acid were used. Arsenic concentrations were determined by flame atomic absorption spectroscopy (FAAS, Varian Spectra AA 200 HT) using acetylene/nitrous oxide flame (performed in the Geological Laboratories, Faculty of Science, Charles University, analyst O. Šebek). The pH of selected solid samples was measured in the leachates of distilled water and 1 M KCl (leaching for 24 hours in 1 : 2.5 ratio). A calibrated digital 330/SET-2 WTW pH-meter with combined SenTix 21 electrode at 21 ^{o}C was used.

4.4. Results and discussion

4.4.1. Mineral identification and description

The ore concentrate material is finely milled. The grain size varies from several micrometres to c. 200 micrometres. The distribution of both main ore minerals (arsenopyrite and löllingite) is random. Pyrite was found as a locally common accessory, and occasional cassiterite and native bismuth inclusions were detected in arsenopyrite grains. Only quartz and feldspars were identified as rare representatives of gangue minerals (in amount up to 5 vol.% in the studied samples). The following arsenic secondary minerals were revealed by the XRD, BSE and EDAX study: arsenolite (As_2O_3), scorodite ($FeAsO_4 \cdot 2H_2O$) and the rare mineral kaatialaite ($FeAs_3O_9 \cdot 6\text{-}8H_2O$). In addition, the relatively common occurrence of native sulphur was revealed as well as an occasional, poorly defined phase of Fe-O composition, probably amorphous Fe oxide, associated with decomposed pyrite grains. A more precise specification of this Fe oxide is hindered by its scarcity and intimate intergrowth with scorodite. These secondary minerals occur as powdery aggregates and fragile crusts on the surface of the concentrate body and/or form cement among the primary grains in subsurface parts of the body. For chemical compositions of secondary minerals see Tab. 1.

Table 1. Chemical analyses of secondary minerals from the Přebuz concentrate (EDAX)

Oxides [wt.%]	Arsenolite average value* n=6	Fe oxide average value* n=3	Scorodite without S average value* n=7	Scorodite with admixture of S average value* n=7
SiO_2	n.a.	1.5 (0.1, 1.6)	n.a.	n.a.
S**	0.1 (0.1, 0,1)	0.4 (0.2, 0.3)	-	0.5 (0.3, 0.3)
Fe_2O_3	0.9 (1.0, 0.9)	91.7 (2.7, 91.4)	32.6 (0.6, 32.7)	32.5 (0.5, 32.7)
As_2O_3	95.3 (1.8, 95.3)	n.a.	n.a.	n.a.
As_2O_5	n.a.	11.6 (1.8, 12.5)	49.3 (1.2, 49.2)	49.6 (1.4, 50.3)
Total	96.3 (2.0, 96.1)	105.2 (1.2, 105.9)	81.9 (1.6, 82.3)	82.6 (1.4, 83.0)

Abbreviations: n.a. – not analysed, - – not detected, *values given in parenthesis: standard deviation, median, **measured as element.

Arsenolite often occurs in the form of irregularly terminated grains dispersed within scorodite cement. On the surface and in cavities of the concentrate body, it forms both powdery aggregates and well-developed octahedral transparent crystals (Fig. 2). Various arsenolite morphologies mentioned above point to its probable occurrence in several generations. The measured XRD patterns correspond closely to the published data (PDF No. 36-1490). The chemical composition of arsenolite is relatively constant. The low totals (below 100%) and small amounts of S and Fe in the analyses are most probably a result of contamination of omnipresent scorodite and sulphur.

Kaatialaite found at Přebuz occurs in the form of white tiny acicular crystals and their fragile aggregates (up to 1 mm in size) overgrowing scorodite and arsenolite uniquely on the surface of the concentrate body (Fig. 3). It was not found in polished sections, hence no analyses are available. Its XRD pattern corresponds well with PDF card No. 43-0681 and was presented by Filippi (2001). Confirmation of the kaatialaite occurrence in As-bearing mine tailings (cf. Roussel et al., 2000) extends the list of minerals that can be considered factors influencing arsenic mobility in the environment. This is only the second find of kaatialaite reported from the Czech Republic. The first occurrence (in association with löllingite, scorodite, arsenolite and claudetite) was reported by Ondruš et al. (1997) from the Jáchymov ore district. They reported the presence of sulphuric acid in kaatialaite aggregates, which was proposed as a requirement for their stabilization by these authors. At other world localities, kaatialaite was also described as an oxidation product of löllingite in association with arsenolite and other minor minerals (Raade et al., 1984; Schmetzer and Medenbach, 1986).

Scorodite is the most widespread secondary mineral (both arsenolite and scorodite are also present in samples seemingly non-weathered by macroscopic observations). It usually occurs as cement that fills the space among mineral grains (Fig. 4, 5). On the surface of the concentrate body it occurs in the form of finely crystalline coatings, crusts and earthy aggregates (Fig. 2). Its colour varies between green, grey and light brown. All measured XRD patterns are in good agreement with PDF card No. 37-0468. Scorodite analyses are relatively uniform, regular presence of S determined in strongly weathered samples is evidently related to contamination by native sulphur, originated from decomposed arsenopyrite.

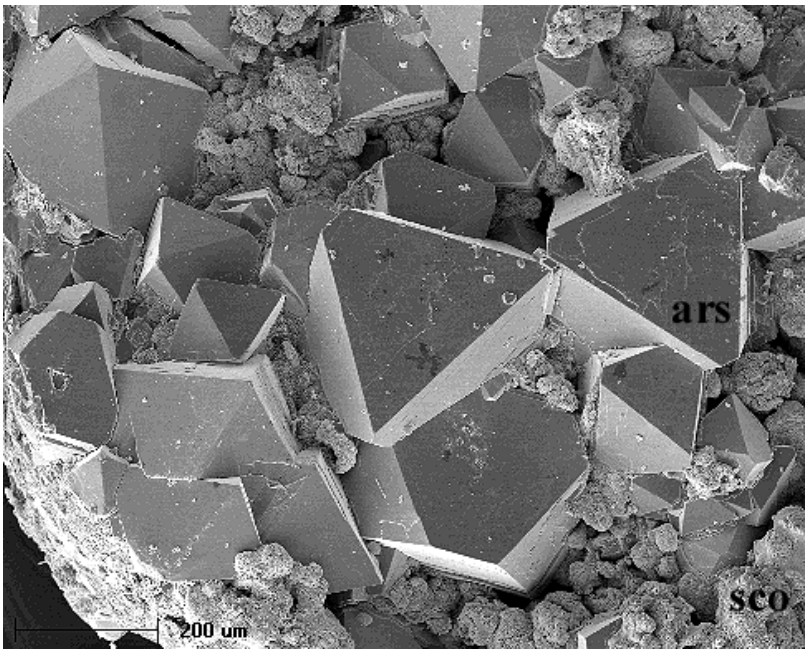

Fig. 2. Octahedral arsenolite crystals (ars) (about 200 micrometres across) associated with powdery scorodite aggregates (sco) growing in a cavity of the concentrate material. SEI photograph.

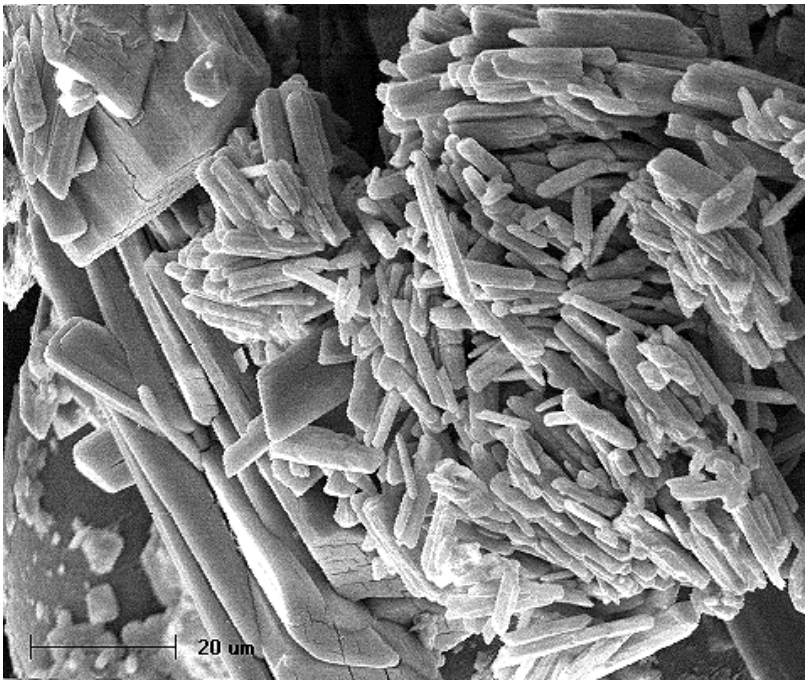

Fig. 3. Aggregate of acicular kaatialaite crystals. SEI photograph.

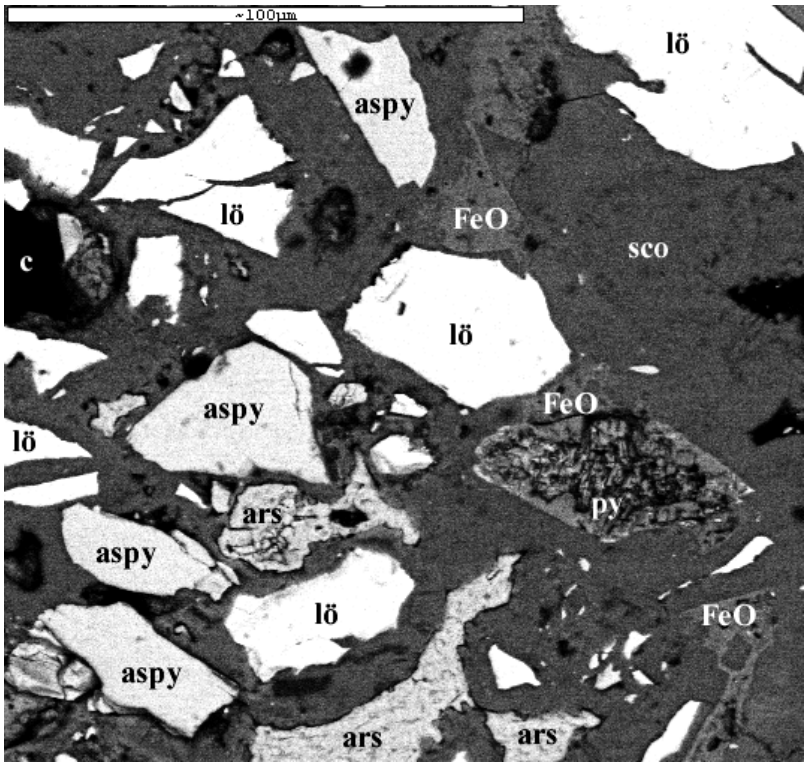

Fig. 4. An example of a slightly weathered sample. Arsenopyrite (aspy) and löllingite (lö) grains are sharply terminated, practically without dissolution features. Secondary cement is composed of scorodite (sco) mass with dispersed arsenolite (ars) grains. Pyrite (py) grain is partly decomposed and associated with secondary Fe-O phase. BSE photograph, scale bar 100 µm.

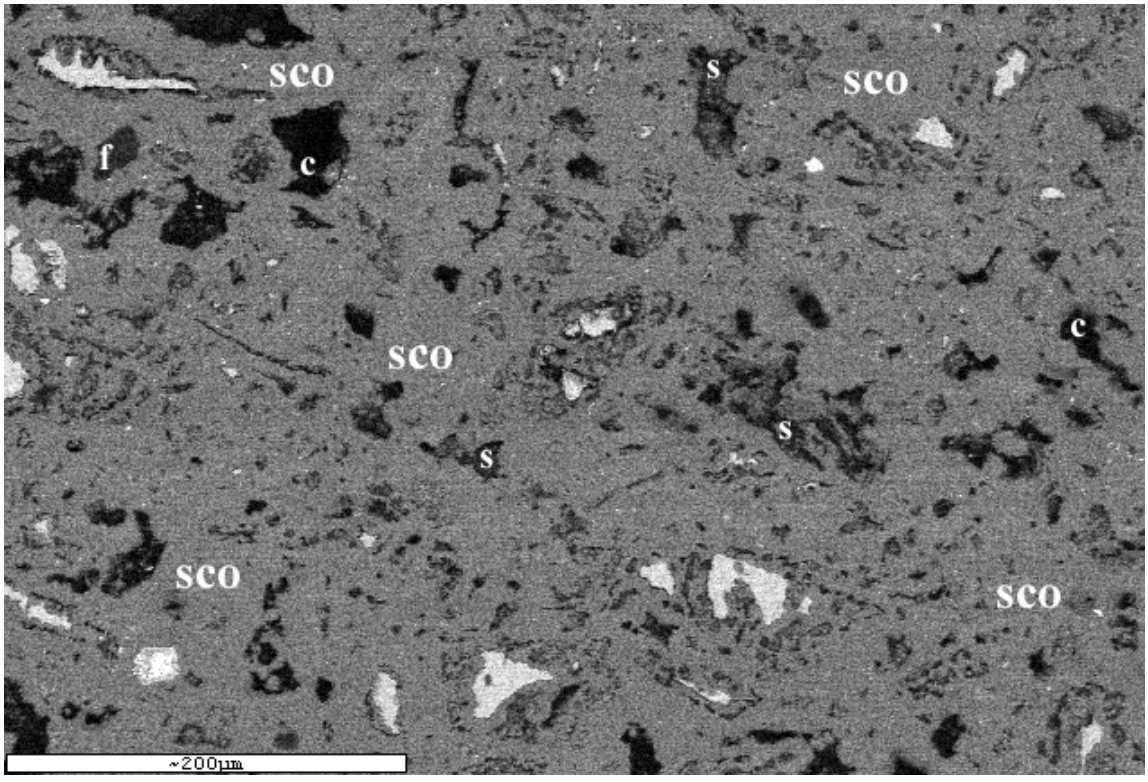

Fig. 5. An example of strongly weathered sample. Löllingite is absent and arsenopyrite grains occur in small relicts only (all white particles in the figure). Secondary cement is composed of scorodite mass (sco) and sulphur (S) that fills some cavities (c) after dissolved arsenopyrite grains. Feldspar occurs as unaffected grain (f). BSE photograph, scale bar 200 µm.

Native sulphur was identified in some XRD patterns (identification according to PDF No. 24-0733) and determined by EDAX. Chemical analyses of sulphur are, however, not included in Table 2 because of the substantial heterogeneity of its aggregates caused by admixture of scorodite, and by its rough surfaces originating from partial filling of cavities following dissolution of arsenopyrite grains (see Fig. 6).

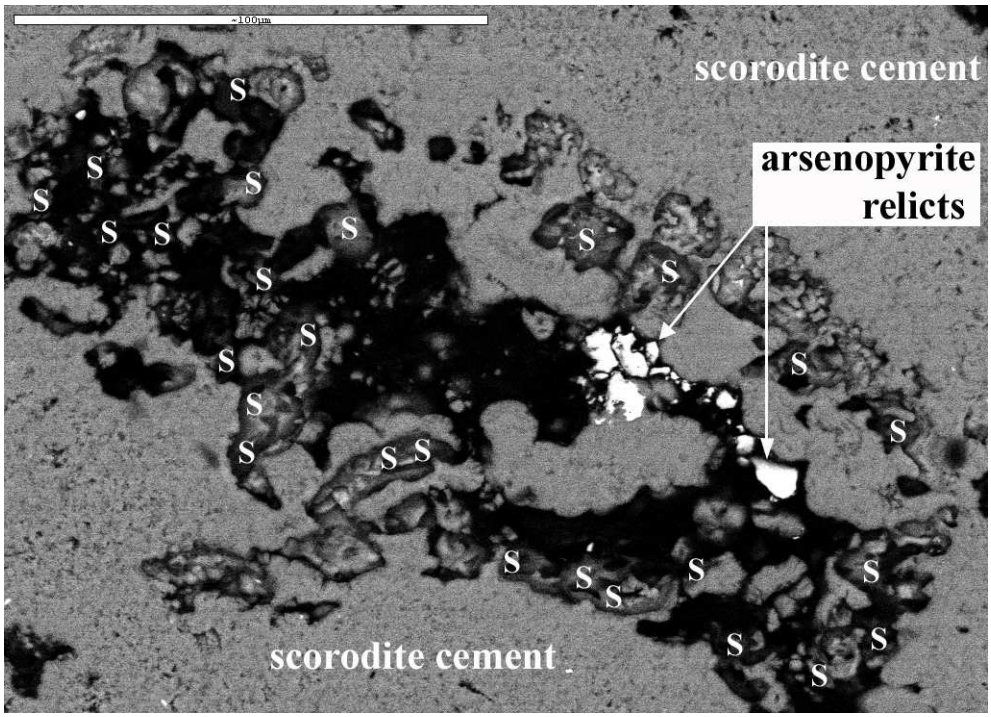

a)

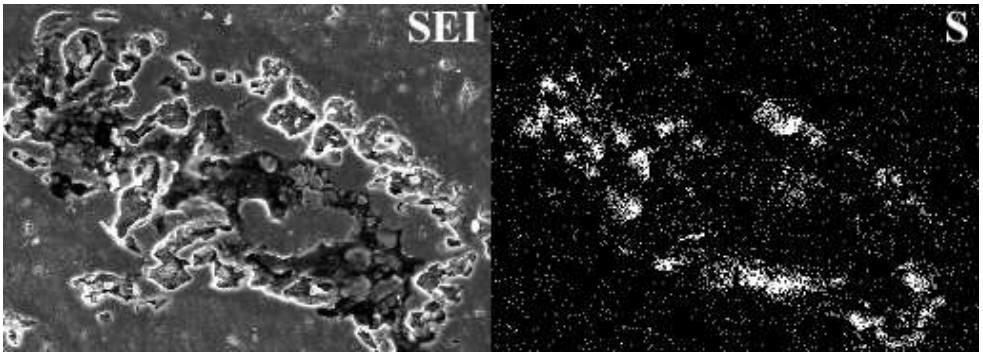

b)

Fig. 6. a) Cavity (all black parts) after practically completely dissolved arsenopyrite (white relicts) in a strongly weathered sample. Relatively homogeneous cement is composed of scorodite. The whole cavity is partly lined by native sulphur (S). Scale bar 100 μm. BSE photograph.; b) Internal structure of the cavity is documented by secondary electron photograph (SEI), and the presence of sulphur is documented by its X-ray distribution analyses (S).

Besides arsenolite, scorodite, and primary arsenopyrite and löllingite, Šrein et al. (1999) mentioned other secondary minerals occurring in the concentrate body, such as bukovskyite [$Fe_2(AsO_4)(SO_4)(OH) \cdot 7H_2O$] and coquimbite [$Fe_2(SO_4)_3 \cdot 9H_2O$]. In their study, however, only routine identification of mineral phases was performed by XRD analyses on mixed samples. Therefore, the identification of mineral phases is not reliable enough, mainly due to the coincidence of diffraction

peaks. However, owing to the assumed extraordinary dynamism of the reactions on the surface of the concentrate, and regarding the possible mineralogical heterogeneity in the body (cf. Chappell and Craw, 2002), some other secondary minerals could occur sporadically.

Table 2. Brief characteristics of the sections sampled near the concentrate body

Sampling site/ layer (depth in cm)	Brief characteristic	General XRD identification	pH (H_2O)	pH (KCl)	As [mg.kg^{-1}]
P1 (situated cca 0.5 m from the concentrate body)					
1 (0 - 5)	dry, coarse, slightly reddish sand 5YR7/2	q, plg, ort, mu	7.68	7.65	1553
2 (5 - 7)	wet, very fine-grained black layer (with clay content/clay-sized particles) 5YR5/1	q, plg, ort, mu, c.m.	7.93	7.68	2580
3a (7 - 21)	dry, medium-grained sand 5YR7/1	q, plg, ort, mu,	7.74	7.56	729
3b (21 - 26)	dry, fine-grained sand 5YR7/1	n.a.	7.80	7.70	1023
4 (26 - 37)	wet, very fine-grained layer generally of dark purple colour 2.5YR4/3; finely laminated (alternation of yellow 10YR8/6, rusty 2.5YR5/8, and reddish colour 10R5/8)	q, plg, ort, mu, c.m.	7.70	7.47	2146
P2 (situated cca 1.5 m from the concentrate body)					
(0-44)	slightly wet sandy soil 7.5YR4/1	q, plg, ort, mu, c.m.	5.55	4.72	13,622

Abbreviations: q–quartz, plg–plagioclase, ort–orthoclase, mu–muscovite, c.m.–clay minerals (not specified).

4.4.2. Oxidation of primary ore and succession of secondary minerals

Oxidation of the present sulphide minerals causes very low pH (the pH measured in H_2O leachates of surface material ranges near 1). Backscattered electron image shows that in such acidic environments löllingite is more susceptible to dissolution than arsenopyrite (see below). This corresponds with the results of Claassen (1993) and Sampson et al. (2000). The studied samples indicate that solutions formed by ore mineral dissolution descended to deeper parts of the body and precipitated there as secondary cement enclosing ore grains, thus slowing down the interior weathering processes (cf. Craw et al., 1999). This is the reason why ore grains in macroscopically slightly weathered samples (from subsurface parts of the concentrate body) show practically no dissolution features although they are surrounded by secondary cement. Initial solutions originating from dissolution of löllingite and partly of arsenopyrite were most probably rich in As^{3+}; and as a result, crystalline arsenolite precipitated among primary ore minerals (arsenolite grains are dispersed in scorodite cement). Later, as the dissolution of arsenopyrite proceeded and the solutions were sufficiently rich in As^{5+} and also Fe^{3+}, scorodite could precipitate (Dove and Rimstidt, 1985; Foster et al., 1998).

Margins of arsenopyrite and löllingite grains dispersed in secondary cement are typically quite sharp in low- and medium-weathered samples, much like those reported by Craw et al. (1999) from their samples from arsenopyrite-bearing tailings. No reaction rims or secondary coatings are visible while pyrite grains are strongly affected by oxidation in these samples. This demonstrates its well-known low stability under acidic conditions (e.g., Alpers et al., 1994). Pyrite was probably significantly dissolved during scorodite precipitation; therefore, the associated Fe oxide occurs as irregular smudges in the scorodite cement and contains significant amount of probably sorbed As.

In strongly weathered samples, pyrite and löllingite grains are absent, therefore only arsenopyrite and gangue minerals occur dispersed in the secondary cement. Partially dissolved larger arsenopyrite grains have rough to serrated margins and are bordered by native sulphur (Fig. 5, 6). Primary smaller grains are present in relicts or are dissolved completely, and small cavities partially filled with sulphur and scorodite remain. Sulphur as the oxidation product of arsenopyrite is well documented (Richardson and Vaughan, 1989; Nesbitt and Muir, 1998), and is also known as the intermediate oxidation product of sulphide ores from natural case studies (Williams, 1990, Ch.3). The characteristic smell of SO_2 at the Přebuz dump clearly demonstrates the presence of sulphuric acid. The common occurrence of sulphur in highly oxidized Přebuz samples is in agreement with the results of Buckley and Walker (1988), who stated in their experiments that arsenopyrite surfaces were enriched by sulphur after oxidation in acidic solutions. Although the biological oxidation by bacteria was not studied, it probably plays an important role in the Přebuz case – cf. Fernandez et al. (1995); and Sampson et al. (2000), who both observed elemental sulphur on the arsenopyrite surface during bacterial oxidation. Arsenolite grains are also often missing in secondary cement of strongly altered samples. It appears that during rainfall this mineral is dissolved and As^{3+} oxidized to As^{5+} (Juillot et al., 1999). Only a thin superficial zone (several mm up to first cm) of the concentrate body and the concentrate fragments along the body were found to be strongly affected by oxidation. Samples from these locations consist predominantly of secondary oxidation products.

A much more complicated situation probably exists on the surface of the body, where kaatialaite, finely crystalline scorodite, and (locally) octahedral crystals of arsenolite were found. Here, conditions must have varied considerably through time: pH changes, biological processes (cf. Sampson et al., 2000), As^{3+} and As^{5+} activity (Williams, 1990, p. 78), total As activity (Vink, 1996), etc. Although the general situation in the studied concentrate may appear simple, it is probably quite complicated on a microscopic scale (cf. Lumsdon et al., 2001) and will change with progressive oxidation.

4.4.3. Arsenic contamination

Arsenolite is characterized as relatively poorly soluble in the water - 37 g/L at 20 °C, but highly soluble in diluted HCl solutions (by the US EPA criterion), while scorodite is much more stable under moderately to strongly oxidizing and acid conditions (Vink, 1996). Major incongruent dissolution of scorodite has been described for higher pH (from ca 5) (Dove and Rimstidt, 1985; Krause and Ettel, 1988), with congruent dissolution at highly acidic conditions - pH between 1.0 and 2.4 (Krause and Ettel, 1988). The very low pH measured on the concentrate surface thus leads to significant arsenic release and consequent contamination of the environment in the vicinity of the concentrate body. Section P1 passes through a heterogeneous anthropogenic material with laminated old tailing pond sediments (mostly of sand composition) at its base. Only tailing pond sediments were sampled. Section P2 passes through old waste pile composed of blocks with sand-sized material containing certain amounts of clay and humus matter. This section shows no stratification; hence only one mixed sample was taken for analyses. For more detailed characteristics of both sections see Table 2.

Small differences in pH(H_2O) versus pH(KCl) leachates (average value 0.13) in section P1 suggest low H^+ ion sorption capacity, thus low contents of organic matter and clay minerals, in contrast to section P2 (average value 0.83). Also particle sizes differ in the individual sections and layers in section P1. Both these aspects have a direct influence on arsenic sorption (e.g., Chunguo and

Zihui, 1988; Cornu et al., 1999; Roussel et al., 2000; Lombi et al., 2000; Lin and Puls, 2000; Bhattacharya et al., 2002). Arsenic concentrations in section P1 range between c. 730 and 2580 mg kg^{-1}, with the highest values determined in a layer 2, which is composed of very fine sand with clay admixture (determined by sieving, and XRD). This layer retains arsenic, so the next layers 3a and 3b show markedly lower arsenic concentrations. Another arsenic enrichment is confined to layer 4, which has again higher clay content and significantly smaller grain size. A much higher arsenic content (13,622 mg kg^{-1}) was determined in loamy material in section P2. Quartz, feldspars and muscovite are the major minerals in all layers as ascertained by preliminary XRD determinations. Accurate specification of clay minerals is not reliable from these types of samples but kaolinite and muscovite/illite appear to be present in the samples.

Further investigation, not planned within the current research, should be performed to specify As binding in the samples studied. Prospective would be some of the sequential extraction methods developed especially for the study of arsenic in soils (e.g., the method of Wenzel et al., 2001).

4.5. Summary and Conclusions

The unique arsenic anomaly at the Přebuz abandoned mine was studied from a mineralogical point of view. Finely milled arsenic concentrate (composed mainly of arsenopyrite and löllingite and accessory pyrite ± small admixture of other minerals) has been oxidizing under exposure to climatic effects for at least 20 years. New secondary minerals scorodite, arsenolite, kaatailaite, native sulphur and probably Fe-oxide precipitate either on the surface of the concentrate pile and/or in the form of cement among the grains of milled material. Highly acidic conditions on the surface of the concentrate body imply dissolution of arsenolite and scorodite, and thus causing contamination of the environment. This presumption is confirmed by arsenic concentrations determined in close proximity to the arsenic body. Successive formation of secondary minerals on the surface as well as low under the surface of the concentrate body was suggested. Pyrite is the first dissolved, then löllingite, and finally arsenopyrite. Secondary cement inhibits the fast oxidation of ore grains in deeper parts of the concentrate body.

Acknowledgement

This research was supported by the project No. 79-502 881 (EMOZMiD), financed by the Rio Tinto Technology Development, and by the project CEZ: No. Z3-013-912. The author would like to thank to Dr. J. Adamovič for reading of the manuscript and Dr. V. Šrein for notice about the locality.

CHAPTER 5. Mineralogical speciation of arsenic in soils above the Mokrsko-west gold deposit, Czech Republic

Michal Filippi[a*], Barbora Doušová[b], Vladimír Machovič[b,c]

[a] *Institute of Geology, v.v.i., Academy of Science of the Czech Republic, Rozvojová 269, 165 00 Prague 6, Czech Republic*

[b] *Institute of Chemical Technology Prague, Technická 5, 166 28 Prague 6, Czech Republic*

[c] *Institute of Rock Structure and Mechanics, Academy of Science of the Czech Republic, V Holešovičkách 41, 182 09 Prague 8, Czech Republic*

Status: Published in journal the Geoderma, 139, 1-2: 154-170

Abstract

Natural soil profiles strongly contaminated by arsenic (As) have been studied. Soils were characterised by its pH, chemical composition, carbonate, humus, exchangeable cations and H^+, and oxalate extractable Fe contents. Mineralogical and chemical speciation of the As was studied by mineralogical methods and sequential extraction. Results were compared and discussed regarding the two different types of soil environment: i) soil developed above the flat unforested granodiorite bedrock and ii) soil developed above the volcanosedimentary bedrock in a sloping forested area. As-bearing minerals were concentrated from soils using heavy liquid and determined using XRD, SEM-EDS/WDS, and Raman spectroscopy. Iron (III) oxyhydroxides (FOHs); K(-Ba) pharmacosiderite, arseniosiderite, scorodite, and jarosite were identified as products of arsenopyrite and/or pyrite oxidation. Arsenates of varying chemical compositions dominate the soil above the granodiorite, while goethite, minor hematite and other indistinguishable FOHs are observed in the soil above the volcanosediments. The diversity and stability of the As secondary minerals in the studied soils are influenced partly by variation in the bedrock composition and mainly by the presence/absence of vegetation cover which mirrors in various contents of exchangeable Ca^{2+}, content of Fe oxalate, and pH. The results of the sequential extraction show an average to high As retention by these soils, when As was extracted during the third and fourth extraction steps (NH4-oxalate buffer, ascorbic acid) in most samples. This finding indicates that As is more mobile in soils where arsenates dominate over well crystallized FOHs.

Keywords: Arsenic speciation; Pharmacosiderite; Arseniosiderite; Scorodite; Iron (III) oxyhydroxide; Sequential extraction

5.1. Introduction

The most important local As inputs into soil and sediments are (except volcanic activity) anthropogenic sources related to mining and ore dressing activities (Nriagu, 1989). Recently, various authors have aimed to understand As behaviour and speciation in soils (e.g., Voigt et al., 1996; Dhoum and Evans, 1998; Corwin et al., 1999; Roussel et al., 2000; Craw et al., 2002; Fukushi et al., 2003; Néel et al., 2003; Ferreira da Silva et al., 2004) with few dealing with soil contamination from natural sources (e.g., Pierrot, 1964; Jacobs et al., 1970; Bowell, 1994; Morin et al., 2002; Pfeifer et al., 2004).

Generally, in mine waste materials and related minesoils, most of the physico-chemical parameters change rapidly and are highly unstable. These materials offer good examples for studying the initial conversion of the primary As minerals into unstable secondary products, and also other interactions caused by As-rich solutions (see e.g., Juillot et al., 1999; Gieré et al., 2003; Paktunc et al., 2004; Salzsauler et al., 2005). In mature soils where contamination arises from natural sources (e.g., in supergene environments of the ore deposits) the time of geochemical evolution is much

longer than in mine waste materials. It can therefore be assumed that a geochemical equilibrium has been established and the geochemical/mineralogical conditions are considered to be stable for greater periods. Mature contaminated soils could therefore be assumed to be the end point of the unstable/transient systems. Such account calls for the study of these soils from all aspects.

Previous work has been carried out to compare As mineralogical speciation at various sites of different ages (Filippi et al., 2004). This study revealed the need to investigate soils in greater detail. Current research was concentrated on the Mokrsko locality, because of the extensive geological knowledge and the high As content in natural soils. The three main objectives for the present study were: i) to determine the mineralogical speciation of As and the minerals that occur throughout the soil profiles; ii) to verify the relationships between selected pedological parameters and As-bearing secondary minerals; and iii) to test a representative sample of sequential extractions and compare this data with knowledge from mineralogical studies. These aims should be pursued above all with respect to the supposed dissimilarity of the soils above the granodiorite and those above the volcanosedimentary bedrock.

5.2. Site description

The village of Mokrsko is located in central Czech Republic (Fig. 1), between 400 and 488 m above see level, annual precipitation is 500-550 mm per year (pH 4.5-4.7), and the average temperature is 7.8 oC (data from the Czech Hydrometeorological Institute). The Mokrsko-west mesothermal gold deposit is a regular sheeted veinlet system composed of quartz veins which varies between 100-300 m thick (Morávek et al., 1989). The deposit is hosted by a biotite - amphibole granodiorite of Variscan age, extending across the contact into the Upper Proterozoic volcanosedimentary complex, which is metamorphosed in greenschist facies (Fig. 1). The granodiorite is relatively unaltered by hydrothermal processes, therefore the primary ore mineralisation is not affected by transformation to secondary minerals. The mineralisation is represented by quartz with relatively common calcite and minor chlorite, biotite, amphibole, microcline, and other minerals. The total amount of sulphides is < 5 % vol. (Morávek et al., 1989). Arsenopyrite (FeAsS) is the most common sulphide in the ore and is the main source of As contamination in the area.

Cliff and Morávek (1995) estimated the general level of As in the ore to be 300-500 mg/kg. The extent of As pollution in the fields and meadows of the Mokrsko gold deposit area indicates that levels of As in soil are >200 mg/kg over an area of approximately 112 ha, >500 mg/kg over approximately 30 ha, and >1000 mg/kg over approximately 13 ha (Morávek et al., 1989; Drahota and Pertold, 2005). Jílek (1985) analyzed the groundwaters of Mokrsko village, and found that levels of As were as high as 1.69 mg/L (median 0.59 mg/L), considerably above the Czech norm for drinking water (0.05 mg/L). The pHs of the groundwaters vary between 6.81 and 8.20; Ca-HCO3-SO4 and Ca-Na(Mg)-HCO3 were the most common determined types of analyzed waters (Jílek, 1985; Drahota and Pertold, 2005, respectively).

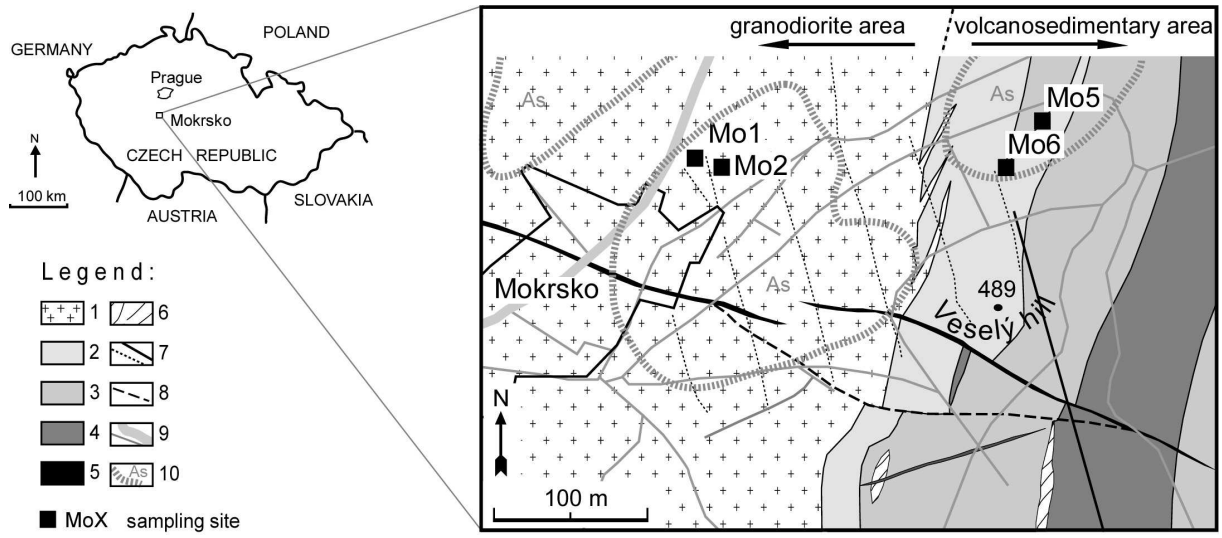

Fig. 1 Location of the Mokrsko-west deposit and simplified geological map of the area (adjusted after Morávek, 1996). Legend: 1– amphibole-biotite granodiorite; 2 – shales; 3 – intermediate tuffs; 4 – intermediate and mafic volcanics; 5 – basic dyke rocks; 6 – barite dykes; 7 – surface prospecting from 80s´ (dashed line), gallery; 8 – fault; 9 – forest ways (thin line), road; 10 – approximate areas with high contents of As in soil (>1000 mg/kg).

5.3. Sampling and analytical methods

5.3.1. Soil sampling and characteristics

Sampling sites were selected on the basis of the following: those which were evolved from the previous geochemical prospecting and exploration works (Janatka and Morávek, 1990); high contents of As; thin soil cover so as to reach the complete depth of the soil profiles; and finally to reach both types of bedrock which are granodiorite and volcanosediments. Soil samples were taken by a combination of trenching, hand auger drilling, and down-hole (non-rotational) hammer drilling. Profiles Mo1, Mo2, Mo5 and Mo6 were sampled in small vertical segments. Macroscopic characterisation of the horizons was published by Filippi et al. (2004). Horizons that were particularly distinguishable were classified according to Driessen et al. (2001) with the schematic description presented in Figure 2. Profiles Mo1, Mo5 and Mo6 were classified as a Haplic Cambisol, and profile Mo2 a Leptic Cambisol according to the FAO system (FAO, 1998). Profiles Mo1 and Mo2 were sampled from a morphologically flat agricultural field overlying granodiorite bedrock. Profiles Mo5 and Mo6 were sampled from a sloping area forested with a variety of spruces and deciduous trees overlying volcanogenic and sedimentary rocks of Proterozoic age.

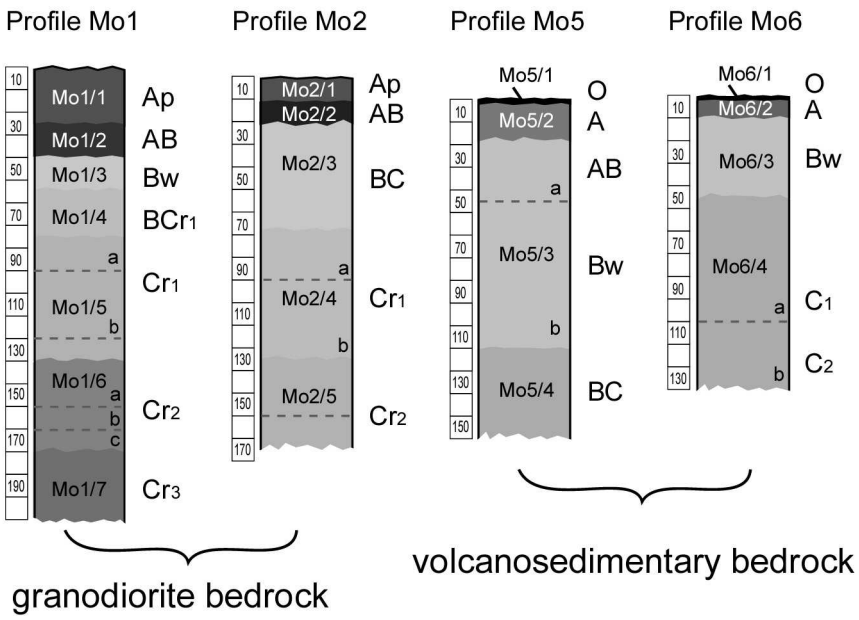

Fig. 2 Soil profiles and location of the samples. For description of horizons see Appendix in Filippi et al. (2004)

5.3.2. Preparation of the mineralogical samples

Samples were air dried at room temperature and sieved to 2 mm. Samples were then prepared in three different ways: natural samples, samples concentrated by panning in denatured alcohol and samples concentrated in heavy liquid. Samples were washed in denatured alcohol to remove the clay fraction, and to separate aggregates. Panning and heavy liquid were used to concentrate the medium and heavy mineral fractions, where the Fe- and As-bearing minerals were expected. The concentrated samples were then sieved into several grain fractions (2-0.5 mm, and 0.125-0.5 mm) and thin- and polished sections were produced. Several grains were also selected by hand under the binocular microscope for analysis by X-ray diffraction, Raman and scanning electron microscope (SEM).

5.3.3. Semi-quantitative bulk chemical composition

Samples (0.8 g finely milled and compacted into tablets) from the upper and lower parts of selected profiles from the granodiorite and volcanosedimentary bedrock were analyzed by X-ray fluorescence (XRF) employed an ARL 9400 XP+ spectrometer under the following conditions: voltage 20-60 kV, probe current 40-80 mA; effective area 490.6 mm^2. UniQuant software was used for data evaluation.

5.3.4. Pedological characteristics

Selected pedological characteristics were determined in samples throughout soil profiles to further characterize the soils overlying the unforested granodiorite and the forested volcanosediments. Exchangeable base cations Ca^{2+}, K^+, Na^+ and Mg^{2+} were extracted from soil by leaching with 0.1 M barium chloride ($BaCl_2$) buffered at pH = 8.1 (Buurman et al., 1996) and determined in the leachate by atomic absorption spectrophotmetry, (AAS; Varian SpectrAA 300). For exchangeable H^+ determination Mehlich 3 absorption was used (Mehlich, 1985). For carbonate content samples were

leached in HCl and the volume of released CO_2 was determined volumetrically. The humus content was calculated by the Cox method (content of burnable carbon determined by sulfochromic oxidation): Cox $\times$ 1.7 constant. Free forms of amorphous Fe oxides (dissolvable in oxalate) were determined according to the methodology of Tamm (extraction by ammonium oxalate, AAS determination) (Buurman et al., 1996). Determination of cation exchange capacity (CEC) was also performed using $BaCl_2$ solution buffered at pH = 8.1. The pH was measured in the leachates consisting of distilled water and 1M KCl solution (leaching for 24 hours, ratio of 1:2.5). A calibrated digital WTW 330/SET-2 pH-meter was used with a SenTix 21 combined electrode at 21 ^oC.

5.3.5. Separation in heavy liquid

To investigate the secondary minerals in a soil, a sufficient amount of mineral grains are necessary. The previous preliminary investigation performed on four extremely contaminated soil samples revealed presence of K(-Ba) and Ca-Fe arsenates as well as ferric oxyhydroxides (FOHs) (Filippi et al., 2004). These minerals and other related minerals have a specific gravity greater than 2.8 $g.cm^{-3}$. Separation was performed on 5 g of 0.25-0.125 mm fraction by bromoform ($CHBr_3$) diluted with 1,4-dioxan ($C_4H_8O_2$) solvent (specific gravity 2.81 $g.cm^{-3}$). The efficiency of the procedure was verified on both heavy and light fractions by binocular microscope observation and by X-ray diffraction.

5.3.6. X-ray diffraction analyses

X-ray diffraction analyses (XRD) employed PHILIPS X´Pert PW 3710 and X´Pert Pro diffractographs under following conditions: CuKα radiation, graphite secondary monochromator, 35 to 40 kV, 30 mA, step scanning at 0.01 and 0.05^o/3s in the range of 2-60^o or 2-90^o 2θ. The ZDS, version 6.01 (Ondruš, 1993), the X´Pert HighScore 1.0 d (PANalytical B.V.) software and the powder diffraction database PDF-2 were used for peak identification. Selected individual grains of secondary minerals, separated according to their different surface morphology and colour were analyzed by Debye-Scherrer powder method. The 114.6 mm chamber and Cu/Ni and Co/Fe radiation were used for measurements. Time exposures were from 19 to 25 hours. Recorded powder diffraction data were evaluated using the program POWDERCO in the Excel editor. Calculated values of interplanar spacing were interpreted using the ZDS software and the PDF-2 database. For XRD analyses the high biotite content in heavy mineral fraction in samples from profiles Mo1 and Mo2 were partly eliminated by mechanical manual separation. The separation was carried out by carefully spilling the concentrates from a sheet of paper several times. The biotite occurs as tabular laminae and remains on the paper due to friction and static, while rounded grains of other minerals roll off.

5.3.7. Raman spectroscopy

Raman spectra were collected using the LabRam HR system (Jobin Yvon) equipped with an Olympus BX 41 optical microscope. An objective of 100$\times$ was used to focus the laser beam on the sample placed on an X-Y sample stage. The 532.2 nm line of a diode laser (Model Compass 315M) was used for excitation. Possible thermal destruction of the samples (melting of the sample, deformation of the spectra) was eliminated by measuring samples with a spectra acquisition under 0.5 mW and a counting time of 10-25 sec; thirty accumulations were then combined to obtain a spectrum. Scattered light was analyzed by spectrograph with holographic grating (600 $gr.mm^{-1}$), slit width 150

μm and opened confocal hole (1000 μm). Adjustment of the system was regularly checked using a silicon standard and by measurement in the zero-order position of the grating. An air cooled multicanal CCD camera was used as a detector.

5.3.8. SEM and microprobe study

Chemical composition and micromorphology of mineral grains were studied on a JEOL JXA-50 electron microanalyzer with an EDAX PV 9400 energy-dispersive X-ray analyzer (EDAX). Element distribution was mapped by EDAX with a counting time of 20 minutes for each element. Accurate electron microprobe analyses (EMPA) were performed by wavelength dispersion spectroscopy (WDS) on a CAMECA SX100 microanalyzer. Polished sections were coated with carbon for chemical analyses and backscattered electron imaging and mineral grains were coated with gold for micromorphology analysis. Operating conditions were as follows: voltage 15-20 kV, beam current 10-14 nA and counting time 60 sec for the whole analyses on the EDAX and 10 sec for each element on the WDS. The following standards were used for measurements on both the EDAX and WDS: barite (Ba, S), diopside (Ca, Si), GaAs (As), hematite (Fe), jadeite (Al, Na), leucite (K), MgO (Mg), TiO_2 (Ti), spinel (Mn). Correction procedures for atomic number, absorption and fluorescence effects (ZAF) were applied for the calculation.

5.3.9. Sequential extraction

The sequential extraction according to Wenzel et al. (2001) evolved especially for As speciation in contaminated soils, was selected for purpose of this study. Small adjustments including the use of $(NH_4)_2HPO_4$ solution in the 2nd step, and pH treatment of extraction agents with 1 M HCl (according to Keon et al., 2001) in the steps 3 and 4 were made. The concentration of As in the aqueous samples was measured by UV/VIS spectrophotometry (UNICAM 5626). The amount of As(V) was determined by the molybdenum blue method at 825 nm (Malát, 1973; Haywood and Riley, 1976). This method allows the required concentration range to be controlled due to the readily changeable and precise calibration. Unfortunately, it is inapplicable for the phosphate leached samples from the step 2. Therefore, the concentration of As in solutions derived from this step was analyzed by AAS (VARIAN SpectrAA 300) equipped with a VGA 76 hydride system (As detection limit = 0.5 ppb). The accuracy of obtained results was verified by inductively coupled plasma optical emission spectrometry (ICP-OES, IRIS Intrepid II instrument, model XSP DUO; detection limit for As was 3 ppb) with deviation of 1.5 up to 10 %, depending on the measured As concentration.

5.4. Results

5.4.1. Soil characteristics

XRF analyses of eight samples from all studied profiles are shown in Table 1. Contents of P_2O_5, MnO, BaO, and partly also TiO_2 are low and relatively constant. Small variations in the contents of oxides arise from the variation of primary accessory minerals in the bedrock. Contents of SO_3 are very low in the profiles Mo1, Mo2 and Mo6, and only slightly higher in the Mo5. Somewhat larger values of other oxides including: Na_2O, MgO, Al_2O_3, SiO_2, K_2O and CaO were observed. These variations could be explained by the heterogeneity of the main rock-forming minerals in most samples (see Section

4.2.1.), and in sample Mo1/6b by the large amounts of secondary minerals (see Section 4.2.3.). Contents of Fe_2O_3 are higher in the lower parts of all studied profiles compared with the upper ones. In addition, sample Mo1/6b exhibits a considerable enrichment of Fe_2O_3 as well as As_2O_5 compared to other samples.

Values of the determined pedological parameters are listed in Table 2. All the samples studied have carbonate concentrations below the detection limit (0.1 %) and are therefore not included. The Mokrsko soils can be classified as very low calcic (all classifications in this Section according to Tomášek (1990)). Based on pH(KCl) the soil above the granodiorite can be classified as slightly acid, while soil above the volcanosediments are highly acid. The highest values of the humus contents were observed in the upper parts of the profiles; high to intermediate in profiles Mo5 and Mo6, and low in profiles Mo 1 and Mo2. The values of most of the other horizons are very low (<1 %). Higher contents of exchangeable H^+ in the upper parts of the profiles correspond well with lower pH measured in soil leachates, however in samples Mo1/6b and Mo1/6c increased contents are evident, and will be discussed later. In general, the values of exchangeable H^+ are considerably higher throughout the profiles from soil above volcanosediments, compared to those developed above the granodiorite.

Table 1. Semi-quantitative bulk chemical composition (XRF) of soil samples

Sample / wt.%	Mo1/3	Mo1/6b	Mo2/3	Mo2/5b	Mo5/2	Mo5/4	Mo6/2	Mo6/5	range	mean
Na_2O	2.58	0.73	2.48	2.75	2.42	2.09	1.88	1.39	0.73–2.75	2.04
MgO	1.31	0.61	1.89	2.40	1.40	2.06	1.92	3.18	0.61–3.18	1.85
Al_2O_3	16.83	8.42	18.73	19.43	15.58	18.29	16.60	17.83	8.42–19.43	16.46
SiO_2	69.43	52.01	63.23	59.31	70.29	60.64	67.29	59.63	52.01–70.29	62.73
P_2O_5	0.072	0.11	0.10	0.14	0.19	0.26	0.30	0.38	0.07–0.38	0.19
SO_3	0.0011	0.028	0.0012	<0.001	0.452	1.280	0.120	0.075	0.0011–1.280	0.24
K_2O	2.09	1.62	2.13	1.86	1.32	2.26	1.31	1.65	1.31–2.26	1.78
CaO	2.33	3.74	3.05	4.50	1.41	1.45	1.59	2.34	1.41–5.50	2.55
TiO_2	0.50	0.19	0.64	0.73	0.56	0.60	0.72	1.25	0.19–1.25	0.65
MnO	0.077	0.055	0.11	0.13	0.061	0.073	0.12	0.22	0.06–0.22	0.11
Fe_2O_3	4.41	18.11	6.86	8.17	5.88	10.17	7.70	11.39	4.41–18.11	9.09
As_2O_5	0.18	14.10	0.53	0.40	0.17	0.39	0.16	0.30	0.16–14.10	2.03
BaO	0.11	0.083	0.11	0.082	0.16	0.26	0.18	0.14	0.08–0.26	0.14
Total	99.92	99.81	99.86	99.90	99.89	99.82	99.89	99.78		

The amount of free Fe oxides (Tamm) is relatively stable, except in the bottom part of the profile Mo1. There is a notable positive anomaly that also occurs in values of exchangeable Ca^{2+}, K^+, and Na^+. In profiles Mo1, Mo2 and Mo5 the CEC is low and relatively stable, except samples Mo2/5b, and Mo5/1.

Table 2. List of selected pedological parameters of soil samples

Sample	Depth [cm]	pHH_2O	pHKCl	Humus [%]	H^+ [$mmol^+$/ 100g]	Ca^{2+} [$mmol^+$/ 100g]	K^+ [$mmol^+$/ 100g]	Na^+ [$mmol^+$/ 100g]	Mg^{2+} [$mmol^+$/ 100g]	Fe Tamm [%]	CEC [$mmol^+$/ 100g]
Mo1/1	0-25	6.6	5.9	1.88	4.5	10.00	0.56	0.34	0.72	0.32	13.40
Mo1/2	25-40	7.3	6.9	1.60	<0.5	11.92	0.36	0.18	0.68	0.44	13.70
Mo1/3	40-57	7.1	6.4	0.34	1.5	8.87	0.14	0.18	0.37	0.27	10.80
Mo1/4	57-77	7.2	5.7	0.34	1.5	10.68	0.21	0.38	0.99	0.45	12.80
Mo1/5b	90-120	6.7	5.5	0.14	2.0	9.00	0.35	0.25	1.61	0.83	11.50
Mo1/6b	150-160	6.4	5.5	0.07	19.0	22.10	5.38	1.15	1.29	6.07	13.60
Mo1/6c	160-170	6.2	5.2	0.07	12.0	16.65	1.04	0.66	1.07	3.44	12.80
Mo2/1	0-13	6.3	5.3	1.95	3.0	10.25	0.27	0.15	0.48	0.39	12.00
Mo2/2	13-21	6.9	6.3	1.33	1.5	11.92	0.26	0.22	0.82	0.52	13.00
Mo2/3	21-69	6.8	5.6	0.34	0.5	9.73	0.32	0.21	1.00	0.48	11.70
Mo2/4a	69-90	6.9	5.6	0.14	1.5	8.98	0.26	0.15	1.34	0.47	11.90
Mo2/4b	90-127	6.9	5.3	0.07	1.5	10.21	0.23	0.19	1.73	0.50	14.00
Mo2/5b	150-166	6.5	5.0	0.07	1.5	13.64	0.24	0.22	1.86	0.61	17.80
Mo5/1	0-3	4.1	3.5	9.83	28.0	4.06	0.33	0.28	0.96	0.47	32.50
Mo5/2	3-20	4.3	3.6	2.50	15.5	1.25	0.16	0.24	0.39	0.37	13.30
Mo5/3a	20-45	4.6	3.6	1.19	9.0	3.37	0.26	0.18	0.91	0.38	12.80
Mo5/3b	45-110	5.2	4.2	0.76	8.5	5.96	0.41	0.21	1.66	0.53	12.50
Mo5/4	110-150	5.6	3.6	0.28	2.5	8.17	0.47	0.17	2.45	0.62	14.70
Mo6/1	0-2	3.9	3.2	8.84	33.5	2.20	0.20	0.23	0.90	0.69	28.90
Mo6/2	2-10	4.0	3.3	3.90	29.5	0.63	0.25	0.16	0.54	0.71	26.60
Mo6/3	10-45	4.9	3.6	0.34	11.5	7.26	0.46	0.12	2.64	0.44	20.10
Mo6/4a	45-100	5.7	5.2	0.14	5.5	16.71	0.53	0.15	4.24	0.66	25.80
Mo6/4b	100-130	5.0	3.8	0.83	8.5	15.13	0.60	0.19	3.96	0.60	28.10

5.4.2. Identification and characterisation of the As-bearing secondary minerals

5.4.2.1. Preconcentration and mineralogical composition of the concentrate samples

Heavy mineral fractions were concentrated from nineteen samples representing horizons from all the studied profiles. Several types of mineral grains were distinguished according to colour and surface morphology (Fig. 3). The XRD of mixed concentrate samples confirmed dissimilarity in the secondary mineral distribution throughout the profiles (cf., Figs. 4a and 4b). Generally, the concentrates contain amphibole, biotite, and a portion of feldspars, minor amounts of several accessory minerals and approximately 5 – 70 vol.% of As secondary minerals or FOHs (Table 3). In the light mineral fraction only quartz, feldspars (most often plagioclase) and occasionally minor amounts of biotite or amphibole were identified. Neither arsenic nor other secondary minerals were identified.

Table 3. Frequency of detected secondary minerals found in soils at the Mokrsko locality

Mineral	Selected horizons from upper and from lower part of each profile / Frequency							
	Sample / granodiorite area				Sample / volcanosedimentary area			
	Mo1/3	Mo1/6	Mo2/2	Mo2/5	Mo5/2	Mo5/4	Mo6/2	Mo6/4
arseniosiderite	++	+++	-	-	-	-	-	-
pharmacosiderite	+++	+++	+++	-	-	-	-	+
scorodite	+	++	++	-	-	-	-	-
other unidentified arsenates	+	+	++	-	?	?	?	?
goethite (with As)	+	++	++	+	++	++	+++	+++
goethite (without As)	+	++	++	++	+++	+++	+++	+++
hematite	-	-	+	+	+	++	++	++
other unidentified FOHs	?	?	?	?	?	?	?	?
jarosite	-	-	+	-	++	++	+	++

Explanations for symbols: +++ very common, ++ common, + rare, - not found, ? – possible occurrence

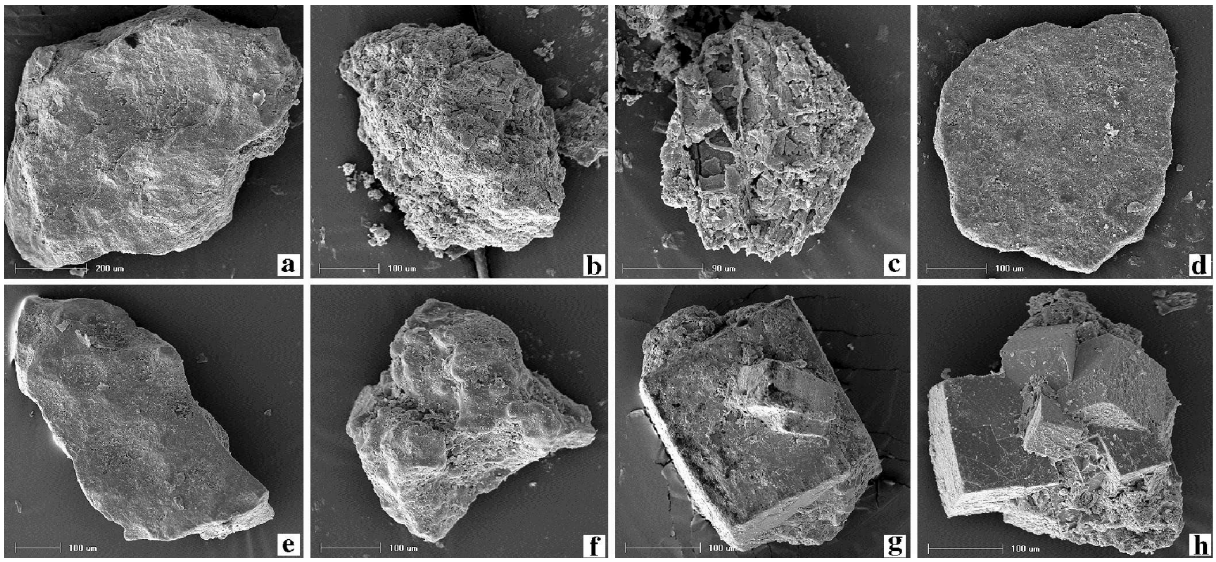

Fig. 3. Typical morphology of various secondary mineral grains (identified by SEM-EDS, XRD, and Raman studies). (a) Dark brown coloured consistent grain composed from pharmacosiderite with admixture of arseniosiderite (sample Mo1/6). (b) Rusty brown incoherent grain composed from mixture of pharmacosiderite with arseniosiderite (Mo1/4). (c) Light brown porous and crumbled scorodite grain (Mo2/3); for XRD pattern see Table 5. (d) Ochre brown homogenous tabular jarosite grain (Mo5/4); for XRD pattern see Table 5 and for internal structure cf., Figure 9l. (e) Compact black goethite grain with smooth surface (Mo5/3); for XRD pattern see Table 5 and for internal structure cf., Figure 9a. (f) Compact black goethite grain with reniform (kidney-shaped) surface (Mo6/3); for XRD pattern see Table 5 and for internal structure cf., Figure 7b, and 7c. (g) Intergrowth of two cubic-like (pseudo)crystals (Mo1/1). (h) Aggregate of perfect cubic-like (pseudo)crystals (Mo6/3); the XRD pattern corresponds to goethite (see Tab. 5 and for internal structure cf., Fig. 9f).

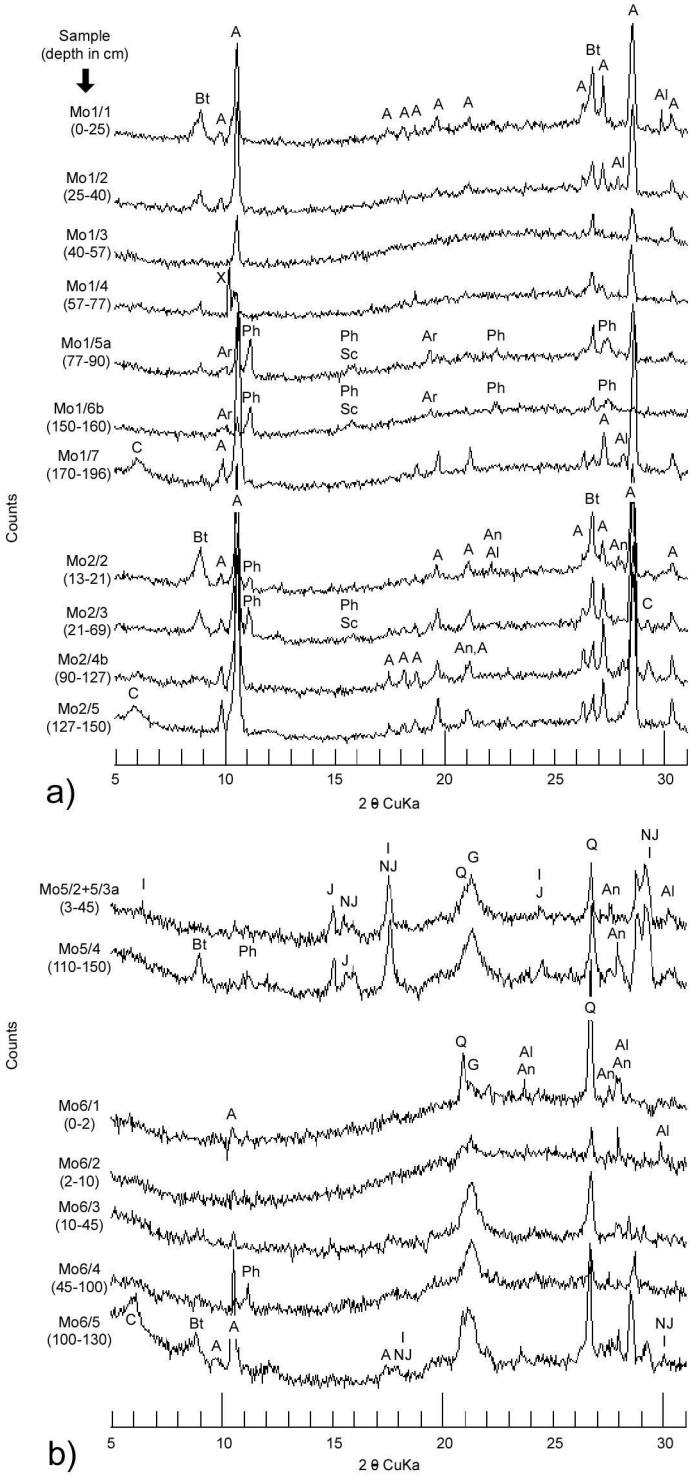

Fig. 4. XRD powder patterns (parts in range 5-31° 2θ) of heavy concentrates obtained from the soil samples above (a) granodiorite and (b) volcanosedimentary bedrock. Key: A – amphibole, Al – albite, An – anorthite, Ar – arseniosiderite, Bt – biotite, C – chlorite, I – illite, J – jarosite, NJ – natrojarosite, Q – quartz, Ph – Pharmacosiderite, Sc – scorodite, X – unidentified peak.

5.4.2.2. Chemical composition of the minerals

More than 160 EDS and WDS analyses were performed to identify As-bearing secondary species present in the Mokrsko soils. The chemical compositions of the analyzed arsenates (except scorodite) and FOHs are variable (Tab. 4). Unfortunately, identification is often complicated due to

chemical heterogeneity of many grains, caused by intergrowths or possible transformations of particular mineral species. However, in Figure 5, there is grouping around the mineral chemical compositions of pharmacosiderite, arseniosiderite, scorodite and possibly yukonite. Selected analyzed grains (n=12), confirmed by Raman spectrometry to be arsenates, have Fe/As molar ratios between 1 and 1.5, which is considered as theoretical range for the common arsenates (Paktunc et al., 2004). The average Ca/As ratio of these grains is 0.24, with the lowest ratio of 0.00 in scorodite and the highest 0.72 in arseniosiderite. Contents of Ca in many pharmacosiderite grains (up to ca. 2 wt.%) measured by WDS points at contamination by arseniosiderite or the presence of some other Ca-Fe arsenate.

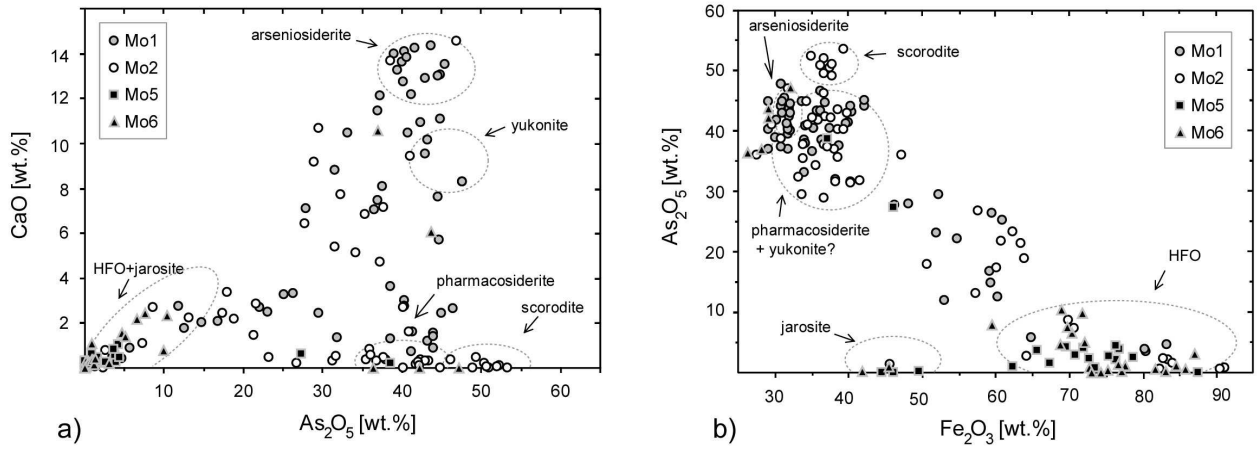

Fig. 5. Chemical composition of secondary minerals. (a) CaO vs. As_2O_5 plot of the studied secondary minerals. (b) Variations of As_2O_5 as a function of Fe_2O_3 in the studied secondary minerals. Dashed circles border approximate areas of theoretical mineral compositions (adjusted according to Paktunc et al., 2004).

As shown in Figure 5 some of the FOHs don't fall into the ferrihydrite or goethite area, although both goethite and hematite were identified by XRD and Raman spectroscopy. Based on EMPA of 12 FOHs grains from granodiorite and 28 FOHs grains from volcanosediments, verified by XRD and Raman spectroscopy, the following contents of the main elements were obtained (in wt.%): Fe_2O_3 (mean 74.14; min 59.40, max. 91.10), As_2O_5 (mean 10.81; min 0.59, max. 26.27), CaO (mean 1.21; min 0.00, max. 3.33), SiO_2 (mean 1.46; min 0.58, max. 2.72); and Fe_2O_3 (mean 78.01; min 65.64, max. 87.00), As_2O_5 (mean 3.14; min 0.00, max. 10.31), CaO (mean 0.65; min 0.06, max. 2.45), SiO_2 (mean 4.58; min 1.63, max. 8.56), respectively.

Jarosite samples analyzed (6 grains) contain levels of As_2O_5 of up to 1.3 wt.% and one sample displays an increased content of Na_2O (2.07 wt.%). Higher contents of Na can be correlated with the results of the XRD study of the concentrate samples, with some peaks corresponding to natrojarosite.

Table 4. Selected electron microprobe analyses of As-bearing minerals (values in wt.%)

Mineral	Horizon	Raman	WDS	Na_2O	MgO	SiO_2	Al_2O_3	K_2O	CaO	Fe_2O_3	MnO	SO_3	As_2O_5	BaO
Pharmacosiderite	Mo1/6	1/15R	1/15	1.66	0.00	0.19	1.13	5.97	1.63	39.95	0.05	0.13	41.29	0.00
		1/27R-1	1/27	5.18	0.00	0.10	0.09	3.64	0.75	39.65	0.00	0.40	41.24	0.00
	Mo2/2	2/6R-2	2/6	1.08	0.02	0.00	0.12	7.79	0.29	38.53	0.00	0.35	43.41	0.08
		2/9R-2	2/9	2.01	0.03	0.13	2.47	7.43	0.35	36.59	0.00	0.04	46.17	0.06
Arseniosiderite	Mo1/6	1/2R	1/7	0.11	0.00	0.49	0.41	0.01	14.09	29.09	0.01	0.00	40.26	0.01
		1/17R	1/17	0.14	0.00	1.22	0.24	0.08	13.63	32.01	0.01	0.22	40.04	0.03
Scorodite	Mo2/2	2/13R-2	2/13	0.04	0.00	0.79	1.48	0.01	0.09	34.87	0.00	0.26	52.22	0.00
		2/17R-2	2/17	0.00	0.00	0.03	0.51	0.03	0.22	37.36	0.00	0.36	50.45	0.02
Goethite and Hematite	Mo5/4	5/1R	5/1	0.05	0.02	1.63	2.59	0.03	0.22	72.70	0.00	0.10	2.31	0.00
		5/14R	5/14	0.02	0.01	4.38	0.40	0.01	0.26	78.68	0.00	0.04	2.41	0.02
	Mo6/4	6/27R	6/27	0.04	0.03	4.90	0.03	0.02	0.06	87.44	0.05	0.14	0.00	0.01
		6/29R	6/29	0.08	0.05	0.85	2.37	0.03	2.32	68.83	0.10	0.22	10.31	0.00
		6/31R	6/31	0.01	0.04	8.56	0.43	0.08	0.10	77.02	0.12	0.01	0.14	0.00
		6/32R	6/32	0.11	0.06	2.21	3.37	0.04	2.20	70.24	0.31	0.65	6.52	0.04
		6/34R	6/34	0.00	0.05	2.84	0.03	0.00	0.06	82.99	0.13	0.18	0.21	0.00
		6/35R	6/35	0.00	0.09	3.59	0.09	0.01	0.14	81.63	0.00	0.13	0.57	0.01
		6/36R*	6/36	0.09	0.14	2.18	3.01	0.01	2.45	69.60	0.01	0.33	7.54	0.00
		6/38R	6/38	0.00	0.12	8.34	3.14	0.05	0.16	75.19	0.05	0.05	0.36	0.00
		6/39R*	6/39[a]	0.03	0.33	35.29	4.28	0.18	1.11	45.48	2.27	0.06	0.95	0.18
		6/46R	6/46	0.00	0.02	2.55	0.08	0.00	0.22	87.00	0.01	0.09	3.06	0.01
		6/47R	6/47	0.02	0.06	4.09	1.28	0.01	0.80	71.66	0.06	0.08	9.87	0.02
		6/48R	6/48	0.05	0.01	7.27	1.68	0.02	0.41	76.62	0.04	0.14	1.34	0.00
		6/49R	6/49[a]	0.01	0.61	16.30	8.25	0.85	0.40	62.58	0.07	0.11	0.46	0.00
Jarosite	Mo2/2		2/26	0.72	0.00	0.03	0.00	6.14	0.07	45.53	0.00	30.35	1.30	0.00
	Mo5/4		5/2	1.04	0.00	0.00	2.35	7.50	0.09	44.55	0.00	29.78	0.06	0.02
			5/13	0.54	0.01	0.02	1.45	4.89	0.13	49.51	0.02	29.32	0.28	0.03
			5/16	2.07	0.01	0.09	3.30	2.80	0.29	46.07	0.00	29.43	0.07	0.07
	Mo6/4	6/37R	6/37	0.28	0.00	0.04	3.33	7.81	0.32	41.77	0.13	28.72	0.20	0.22

For positions of presented WDS and Raman analyses see Figures 7 and 9, respectively. Except for jarosite, only those chemical analyses where minerals are confirmed by Raman spectroscopy are given. ([a] The identification is uncertain due to high fluorescence within the Raman study.; [b] Probable contamination by rock-forming silicate)

5.4.2.3. As-bearing secondary minerals in soils above the granodiorite bedrock

Pharmacosiderite ($KFe^{3+}_4(AsO_4)_3(OH)_4 \cdot 6\text{-}7(H_2O)$) occurs throughout both profiles as brown coloured grains with structurally homogenous surfaces (Fig. 3a), or as infillings and aggregates in quartz, feldspars, and FOHs. It has complex internal ordering, consisting of completely metamorphosed crystals of primary arsenopyrite and from clustering of several types of Ca-K-Fe arsenates (Figs. 6, and 7a, b, c, d). Chemically and structurally more homogeneous pharmacosiderites overgrow rock-forming minerals and fill fractures in them (Figs. 7e, f, g). The size of pharmacosiderite grains ranges from several tens of micrometres up to ca. 3 millimetres. The two most intensive pharmacosiderite peaks (d-spacing in range 7.97 – 8.01 Å and near 4.61 Å, respectively) were identified in several diffractograms from concentrate samples. Some grains were identified by Debye-Sherrer method (Tab. 5). The Raman spectra of pharmacosiderite (Fig. 8a) shows two intensive bands at 886 cm^{-1} and 860 cm^{-1} assigned to the ν_3 (F), and at 830 cm^{-1} assigned to ν_1 (A_1) vibrational modes. The band at 803 cm^{-1} may be assigned to the OH deformation mode (Frost and Kloprogge, 2003). The low wavenumber region of the Raman spectrum of pharmacosiderite exhibits the most intensive band at 475 cm^{-1} assigned to the bending ν_4 (F) mode. The ν_2 bending mode of pharmacosiderite is observed at 381 and 335 cm^{-1}. The bands centered at 137, 279, 244 and 290 cm^{-1} may be assigned to the Fe-O stretching vibrations. The analyzed pharmacosiderites have different

contents of Ca and K. The spectra of individual grains differ especially in the intensities of the ν_1 and ν_3 modes, and in spectral features between 100-300 cm^{-1} the shifts are not distinctive. However, no dependence between the position of spectral bands and content of Ca and K was observed in the samples analyzed.

Table 5. X-ray diffraction lines obtained by Debye-Scherrer camera from a set of mineral grains

Minerals detected from soil above the granodiorite											
Pharmacosiderite				**Pharmacosiderite**				**Scorodite**			
Ref.[a,b]		**Mo2/2**		**Ref.[c]**		**Mo1/6**		**Ref.[d]**		**Mo2/3**	
d (Å)	I/I_0	d (Å)	I/I_0	d (Å)	I/I_0	d (Å)	I/I_0	d (Å)	I/I_0	d (Å)	I/I_0
7.98	100	7.94	100	8.00	90	8.01	80	5.609	80	5.61	90
4.60	40	4.56	30	4.61	100	4.61	100	5.018	35	5.03	40
3.99	30	3.94	30	3.991	25	4.00	50	4.472	100	4.45	100
3.25	50	3.23	40	3.571	20	3.55	20	4.089	30	4.12	40
2.816	50	2.810	30	3.259	70	3.25	80	3.800	30	3.81	10
2.653	16	2.679	10	2.822	65	2.818	60	3.178	90	3.17	60
2.529	30	2.512	10	2.661	35	2.663	30	3.060	35		
2.404	30	2.392	20	2.408	80	2.401	60	2.999	35		
1.877	16	1.863	10	2.303	55	2.298	30	2.596	35		
1.782	20	1.760	10	1.9358	45	1.929	20	2.582	30	2.586	40
Minerals detected from soil above the volcanosedimets											
Goethite								**Jarosite**			
Ref.[e]		**Mo5/4**		**Mo6/3**		**Mo1/1**		**Ref.[f]**		**Mo5/4**	
d (Å)	I/I_0	d (Å)	I/I_0	d (Å)	I/I_0	d (Å)	I/I_0	d (Å)	I/I_0	d (Å)	I/I_0
4.98	12							5.93	45	5.95	60
4.183	100	4.17	100	4.15	100	4.12	100	5.72	25	5.73	20
		3.70	20	3.71	20	3.71	10	5.09	70	5.09	90
3.383	10	3.329	20					3.65	40	3.66	30
2.693	35	2.701	40	2.678	30	2.69	60	3.11	75	3.20	30
2.583	12	2.592	20			2.518	40	3.08	100	3.08	100
2.489	10							2.861	30	2.847	40
2.450	50	2.445	60	2.442	60	2.437	40	2.287	40	2.281	60
2.253	14	2.249	40	2.245	20			1.977	45	1.973	50
2.190	18	2.194	10			2.205	30	1.825	45	1.808	50
1.7192	20	1.716	50	1.7110	40	1.722	20				

Explanations: d (Å) – interplanar spacing; I/I_0 – intensity. ([a] First 10 strongest reference lines are compared; [b] reference PDF card No. 17-0466; [c] reference PDF card No. 34-0155; [d] reference PDF card No. 37-0468; [e] reference PDF card No. 29-713; [f] reference PDF card No. 22-827)

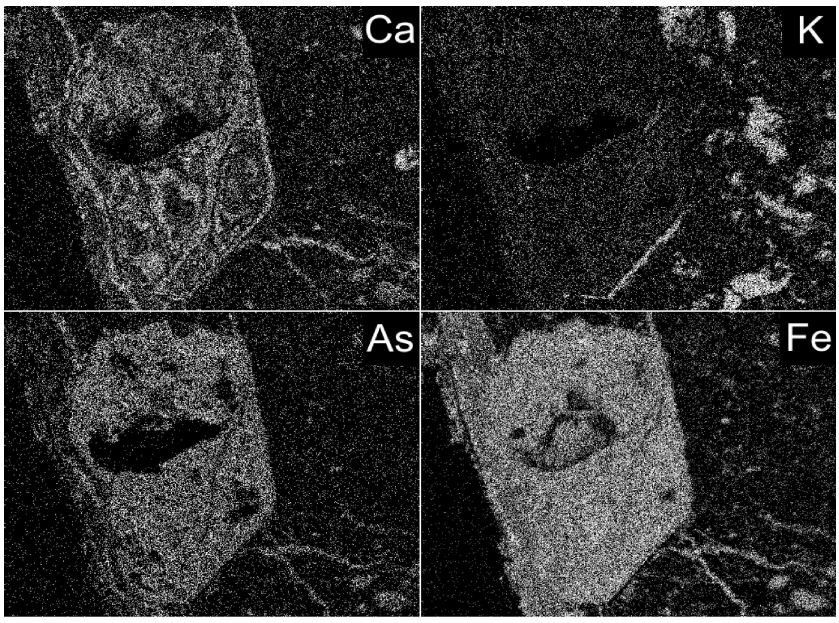

Fig. 6. X-ray mapping of an arsenate grain from Figure 7b, demonstrating heterogeneity in elemental distribution within the bounds of one arsenate grain. Compared to Figure 7b, this section is rotated.

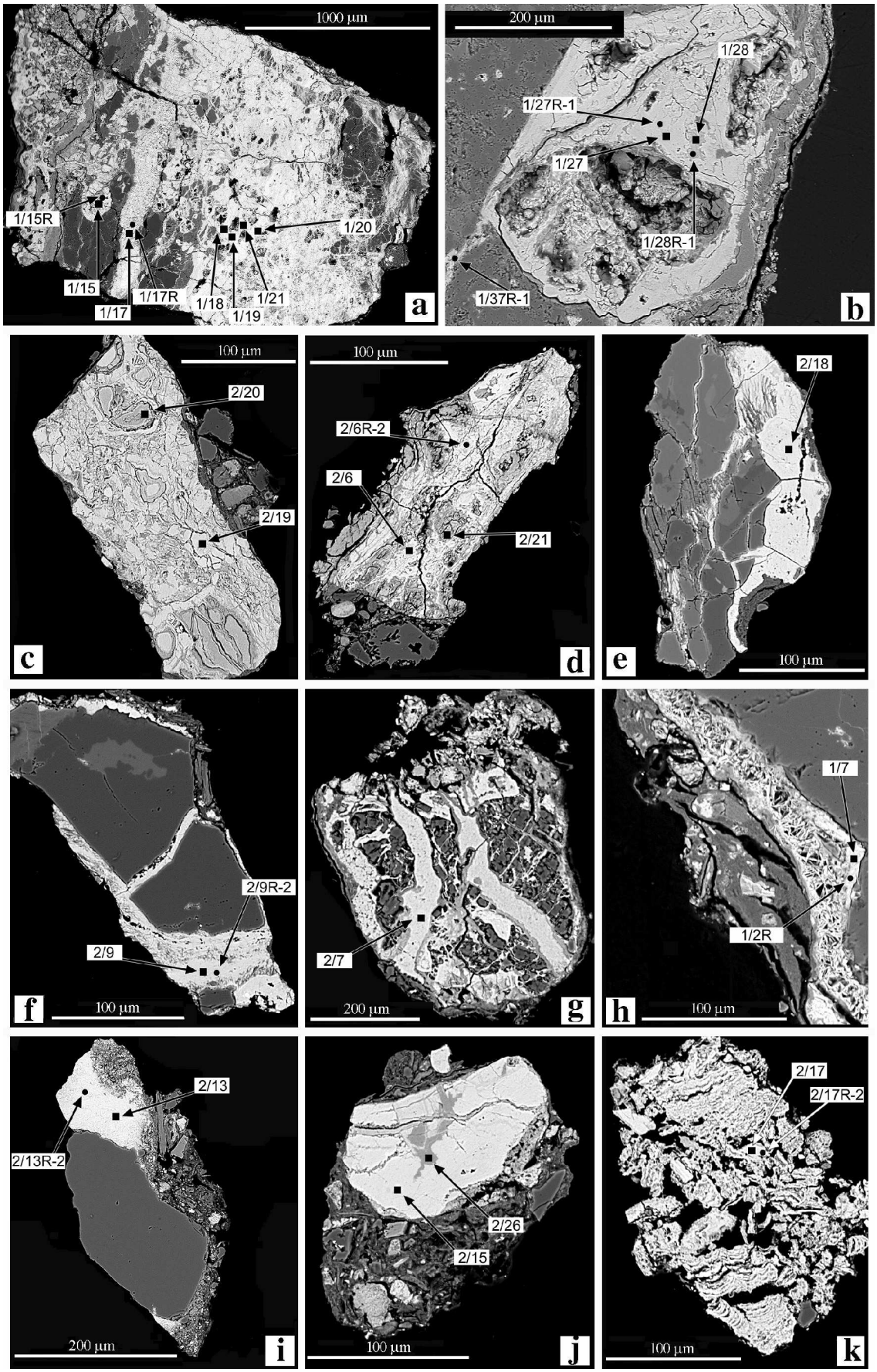
1000 µm
1/15R
1/15
1/17
1/17R
1/18
1/19
1/21
1/20
a
200 µm
1/28
1/27R-1
1/27
1/28R-1
1/37R-1
b
100 µm
2/20
2/19
c
100 µm
2/6R-2
2/6
2/21
d
2/18
e
100 µm
2/9R-2
2/9
f
100 µm
2/7
200 µm
g
1/7
1/2R
h
100 µm
2/13
2/13R-2
200 µm
i
2/26
2/15
100 µm
j
2/17
2/17R-2
100 µm
k

Caption for figure on the previous page:

Fig. 7. Backscattered electron micrographs of different secondary arsenates and other minerals from the soil above the granodiorite bedrock. Black squares and circles point at positions of the chemical (selected representative analyses are given in Table 4) and Raman analyses (selected representative spectra are given in Figure 8), respectively. (a) Complex grain composed from pharmacosiderite, arseniosiderite (lighter phases) and quartz (grey phase). (b) Predominant arsenopyrite crystal metamorphosed by pharmacosiderite (light) in quartz (grey); thin vein in the left corner and leaf-like aggregates near the right margin of the quartz are composed by arseniosiderite. (f), (c), (d) Complex grains composed by pharmacosiderite (lighter) and FOHs (darker). (e), (f), (g) Chemically and structurally homogeneous pharmacosiderites (lighter) overgrowing or replacing rock-forming minerals (darker). (h) Detail of the leaf-like texture of arseniosiderite (lighter) in quartz (darker). (i) Homogeneous scorodite grain (white) aggregated with rock-forming minerals (darker). (j) Scorodite (light) with jarosite (darker inclusion) aggregated with rock-forming minerals (darker). (k) Partly decomposed scorodite grain.

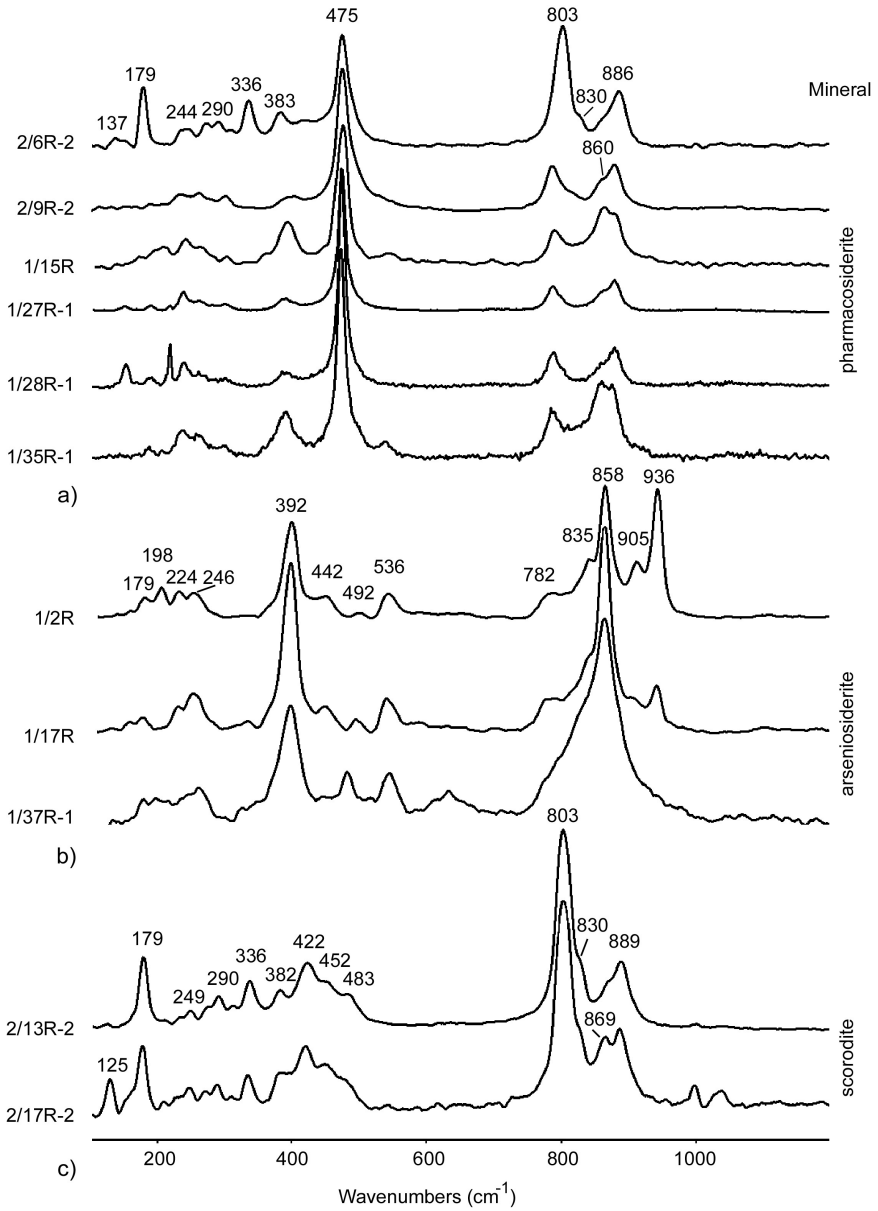

Fig. 8. Set of representative Raman spectra of the studied arsenates in range between 100 and 1200 cm^{-1}. For chemical analyses see Table 4.

Arseniosiderite ($Ca_2Fe^{3+}_3(AsO_4)_3O_2{\cdot}3(H_2O)$) was found primarily in the lower and middle part of the Mo1 profile. Macroscopic arsenate aggregates, which contain major amounts of arseniosiderite, are of rusty brown colour and are unconsolidated and powdery (Fig. 3b). Pure arseniosiderite grains were found only in microscopic scale by SEM-EDS/WDS studies. In some parts of arseniosiderite grains, fuzzy or leaf-like textures were found (Fig. 7h), similar to those observed in arseniosiderite from tailings material studied by Paktunc et al. (2004). The most intensive arseniosiderite peak in diffractograms (d-spacing in range 8.86 – 8.91 Å) of mixed arsenate grains agree with the relevant PDF cards. In the stretching region of the arseniosiderite Raman spectra (Fig. 8b), five bands at 782, 835, 858, 905 and 936 cm^{-1} can be observed. The bands at 858 and 936 cm^{-1} may be assigned to the ν_1 and ν_3 stretching vibrations. The band positions are about 80 cm^{-1} higher in comparison with the stretching band position of scorodite (see below). The most intensive band at 392 cm^{-1} in the bending region has been assigned cautiously to the ν_2 mode, and the band at 536 cm^{-1} to the ν_4 bending mode. Sample 1/37R-1 is probably relatively amorphous as indicated by a broad and poorly resolved band. Several other grains of asreniosiderite were analyzed, but spectra were not obtained due to high fluorescence effects.

Scorodite ($Fe^{3+}(AsO_4).2H_2O$) has been identified less commonly compared to the other arsenates. It occurs mainly in the upper and middle part of the Mo2 profile and to a lesser extent in the lower part of the Mo1 profile. It occurs as separate grains (Fig. 3c) or as intergrowths with rock-forming minerals (Fig. 7i), or rarely with inclusion of As-containing jarosite (Fig. 7j). Scorodite grains are often porous and crumbled, which appear to be partly decomposed (Figs. 3c, 7k). The most characteristic scorodite peaks with d-spacing near 5.61 Å and near 4.48 Å were observed in some diffractograms of the concentrate samples and the identification was confirmed by Debye-Sherrer method (Tab. 5). In the arsenate stretching region of the scorodite Raman spectra (Fig. 8c), two high intensity bands are observed at 803 cm^{-1} (ν_1, symmetry stretching mode) and at 889 cm^{-1} (ν_3, asymmetric stretching mode). The low wavelength region of scorodite is complex. The ν_2 symmetric bending mode can be found at 290 and 336 cm^{-1}, and the asymmetric bending mode at 422 cm^{-1}. The observed position of these bands is in good agreement with the data published by Coleyshaw et al. (1994). The region between 100 and 280 cm^{-1} is probably attributable to the Fe-O stretching vibrations.

Goethite (α-$Fe^{3+}O(OH)$) was observed in three different forms. Single cubic (pseudo)crystals (up to ca. 200 μm in size) assumed to be pseudomorphs of goethite after pyrite were found in samples the upper part of the Mo2 profile (Fig. 3g) with only Fe determined as the major cation by SEM-EDS study. Compact dark brown coloured FOH grains similar to those presented in Figure 3e are found in profile Mo2. This form doesn't contain As and has a steady chemical composition (Tab. 4). The third form of FOH (Figs. 7c, d) was observed by SEM-WDS associated with arsenates as intimate intergrowths or by replacement, and contains significant amounts of As.

5.4.2.4. As-bearing secondary minerals in soils above the volcanosedimentary bedrock

Ferric oxyhydroxides (FOHs) are the most abundant As-containing minerals in profiles Mo5 and Mo6. Although the surface morphology, internal structure and chemical composition of individual grains are varied, goethite determined by XRD and Raman spectroscopy is the predominant mineral phase. Hematite (Fe_2O_3) was occasionally detected by Raman spectroscopy as an admixture in some goethite grains. The following main groups of goethite grains were distinguished:

i) Compact dark brown coloured grains with smooth or bowl-like shaped surface (Fig. 3e). Grains are chemically relatively homogenous and contain small amounts of As. In cross-section grains usually display no visible internal structure or are of a grained-like appearance (Fig. 9a).

ii) Compact dark brown coloured grains often with kidney-like surface (Fig. 3f), sometimes occur as intergrowths with silicates or quartz. In cross-section grains display coloform (Figs. 9b, c, d) or radial fibrous-like structures (Fig. 9e). These types of goethite have variable chemical composition and contain significant amounts of As.

iii) Single cubic (pseudo)crystals and aggregates (Figs. 3h, 9f), similar to those described in the soil above the granodiorite are frequently found in profile Mo6. Raman spectroscopy of several (pseudo)crystals correspond well to a mixture of goethite and hematite (Fig. 10). Grains display a steady chemical homogeneity and an absence of As.

iv) Complex goethites which display different internal structures in cross-section. Reticular, star-like, polygonal and impregnated forms are presented in Figures 9g, h, i, and j. Mixtures of goethite with hematite (e.g., Fig. 9i, g) were also found. Goethite is occasionally associated with indistinguishable FOHs due to a high fluorescence effect observed in the Raman study (e.g., point 6/36R in Fig. 9g), and also as mixtures of FOHs with jarosite (Fig. 9k).

In spite of goethite being considered as one of most stable FOHs in soils, variations in the crystal structure give rise to variability in Raman spectra. The band positions of goethite samples (Fig. 10) at 244, 299, 385, 482, 551 and 684 cm^{-1} are in good agreement with the reported spectra (e.g., de Faria et al., 1997). As mentioned above, hematite was detected in some goethite grains which can be seen in the bands at 225, 298, 409 and mainly 1315 cm^{-1}.

Pharmacosiderite has been found very rarely by SEM-EDS/WDS. It was observed as small grains (tens of microns), intergrown with rock-forming minerals. The main peaks of pharmacosiderite were found in the concentrate sample from the bottom section of the Mo6 profile. Chemical composition of pharmacosiderite from the volcanosedimentary area is characterised by frequent levels of Barium up to ca. 5-10 wt.% (analysis 6/9 in Table 4).

Jarosite ($KFe_3(SO_4)_2(OH)_6$) occurs predominantly as ochre brown coloured platy grains mainly in profile Mo5 (Figs. 3d, 9l). XRD data are given in Table 5 and in Figure 4b. Arsenic containing jarosite was found associated with goethite (Figs. 9c, k). The Raman spectra of jarosite have been extensively investigated by many authors, and the spectrum of jarosite in this work (Fig. 11) is consistent with the published band positions (e.g., Serna et al., 1986) at 1006 cm^{-1} (ν_1 S-O), 1103 and 1153 cm^{-1} (ν_3 S-O), 432 and 451 cm^{-1} (ν_2 S-O), 624 cm^{-1} (ν_4 S-O) and 574 cm^{-1} (γ_{OH}). The low-frequency region exhibits a band of the K, Fe-O bonds.

Caption for figure on the next page:

Fig. 9. Backscattered electron micrographs of different secondary goethites and other minerals from the soil above the volcanosedimentary bedrock. Black squares and circles point at positions of the chemical (selected representative analyses are given in Table 4) and Raman analyses (selected representative spectra are given in Figure 10), respectively. (a) Chemically and structurally homogenous goethite grain. (b) Goethite with coloform internal structure. (c) Goethite with coloform internal structure (lighter parts) associated with jarosite crystals (grey parts – point 5/16) and FOH (dark grey parts – point 5/17). (d) Goethite (lighter) impregnating rock-forming silicates (darker). (e) Goethite displaying radial fibrous-like structure. (f) Pseudomorphs of goethite with hematite after pyrite. (g) Reticular grain composed by mixture of goethite with hematite (light phases) overgrowing unidentified FOH* (darker phase). (h) Mixture of star-like goethite (lighter phases) dispersed in unidentified FOH* (darker phase). (i) Polygonal grain composed by hematite (whiter) and goethite (darker). (j) Goethite impregnation (light phase) in rock-forming silicates (darker phases). (k) Mixture of goethite (white) with jarosite (darker). (l) Single jarosite grain. * The identification was not possible due to high fluorescence within the Raman study.

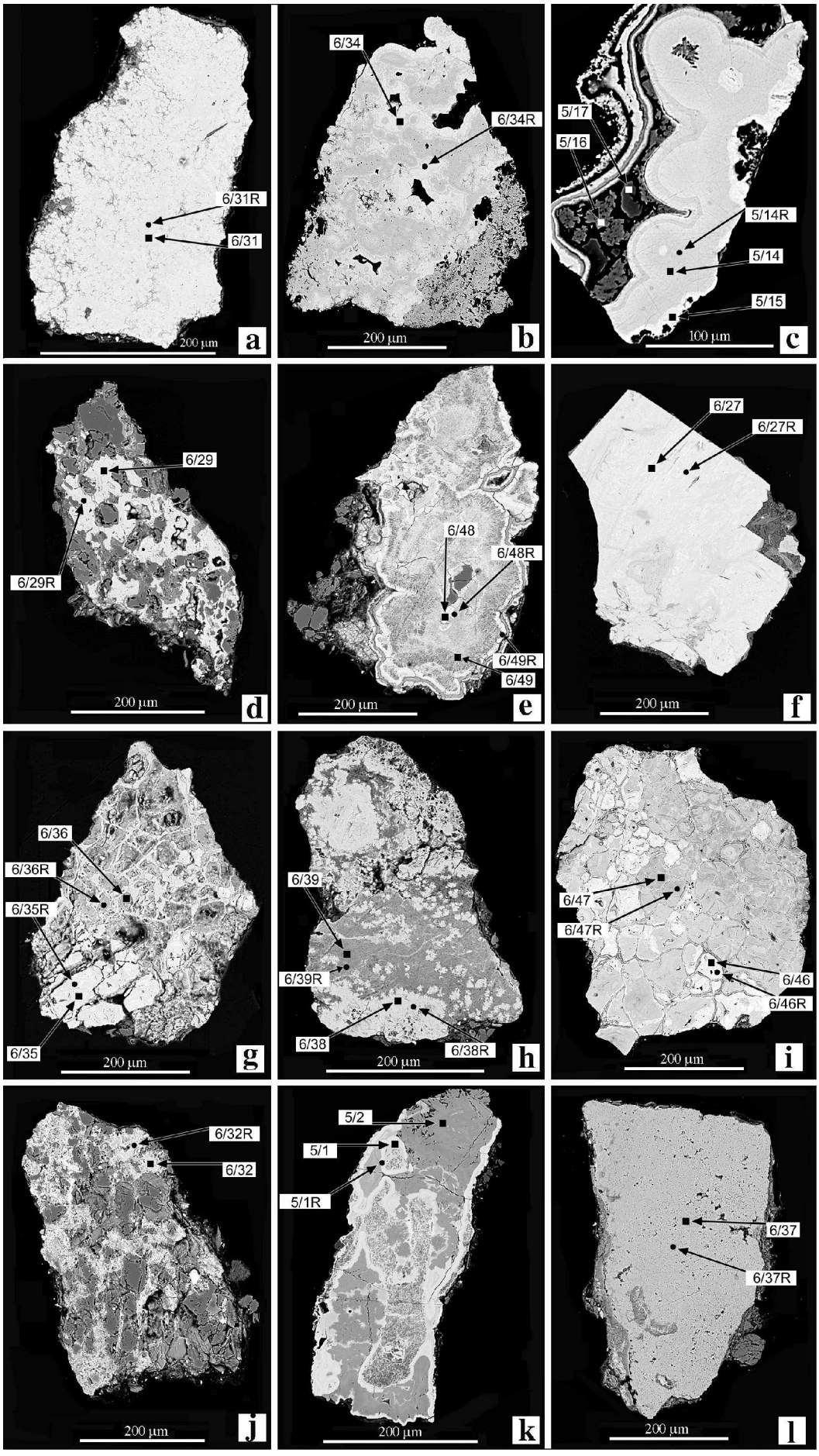
6/31R
6/31
200 µm
a
6/34
6/34R
200 µm
b
5/17
5/16
5/14R
5/14
5/15
100 µm
c
6/29
6/29R
200 µm
d
6/48
6/48R
6/49R
6/49
200 µm
e
6/27
6/27R
200 µm
f
6/36
6/36R
6/35R
6/35
200 µm
g
6/39
6/39R
6/38
6/38R
200 µm
h
6/47
6/47R
6/46
6/46R
200 µm
i
6/32R
6/32
200 µm
j
5/2
5/1
5/1R
200 µm
k
6/37
6/37R
200 µm
l

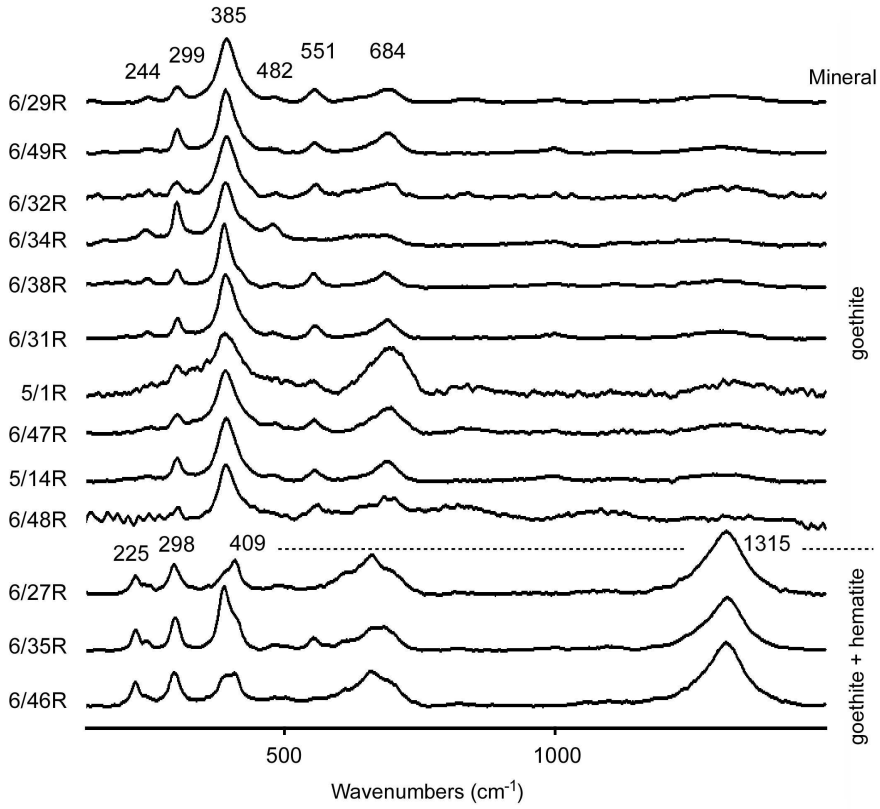

Fig. 10. Set of representative Raman spectra of the studied goethites and hematites in range between 50 and 1500 cm^{-1}. For chemical analyses see Table 4.

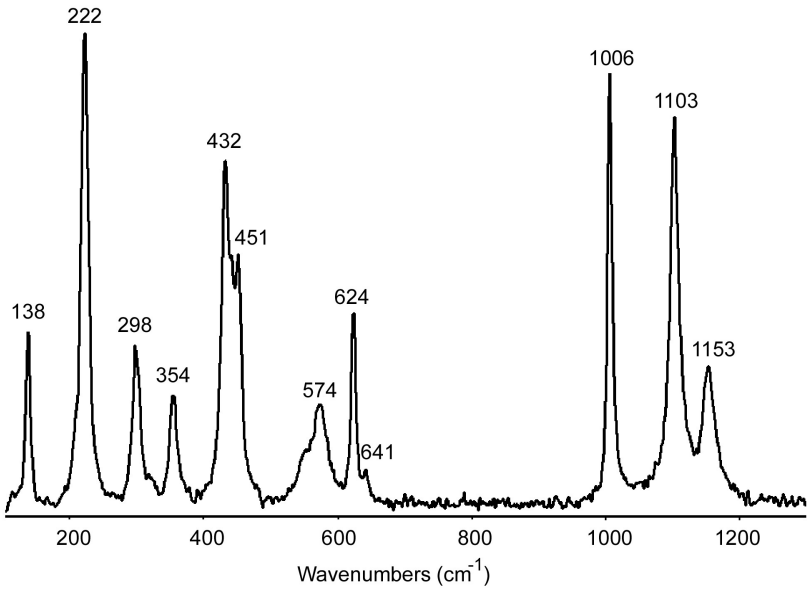

Fig. 11. Representative Raman spectrum of jarosite in range between 100 and 1300 cm^{-1}

5.4.3. Sequential extraction

Results of the sequential extraction are reported in Table 6 in absolute values, and in Figure 12 as the relative As fraction. Three soil samples from profile Mo1 (above the granodiorite bedrock) and three samples from profile Mo6 (above the volcanosedimentary bedrock) have been analyzed as a representatives of both the different petrological settings. The amount of As extracted from first two fractions F1 and F2 is low (up to 3 %), except in sample Mo1/6b, where the value is higher (8 %). The amount of As extracted from the fraction F1, in topsoil samples is high with respect to agricultural land use and calls for other testing. The main part of As was extracted from fractions F3 (ca. 19-53 % and ca. 16-23 % in profiles Mo1 and Mo6 respectively) and F4 (ca. 55-72 % and ca. 75-81 %). Arsenic bound to the residual fraction F5 was not detected in the studied samples, except in a negligible amount in the sample Mo1/6b (1.4 mg/kg), thus fraction F5 is not included in Figure 12.

Table 6. Content of arsenic in particular fractions obtained by sequential extraction procedure (values in mg/kg)

Fraction		**F1**	**F2**	**F3**	**F4**	**F5**	**Σ As**
Sample	**Bedrock**	$(NH_4)_2SO_4$	$(NH_4)_2HPO_4$	$(NH_4)_2ox$	$(NH_4)_2ox$+asc.ac.	$HNO_3+H_2O_2$	
Mo1/1		4.3	23.6	595.9	738.7	n.d.	1,362.5
Mo1/3	granodiorite	1.1	26.7	837.3	718.1	n.d.	1,583.2
Mo1/6b		27.3	1,597	3,467	12,859	1.4	17,951.7
Mo6/1		1.5	19.3	205.5	970.3	n.d.	1,196.6
Mo6/2	volcanosediments	4.4	15.2	198.1	655.0	n.d.	872.7
Mo6/4a		18.8	6.3	464.7	1,976.0	n.d.	2,465.8

n.d. – not detected

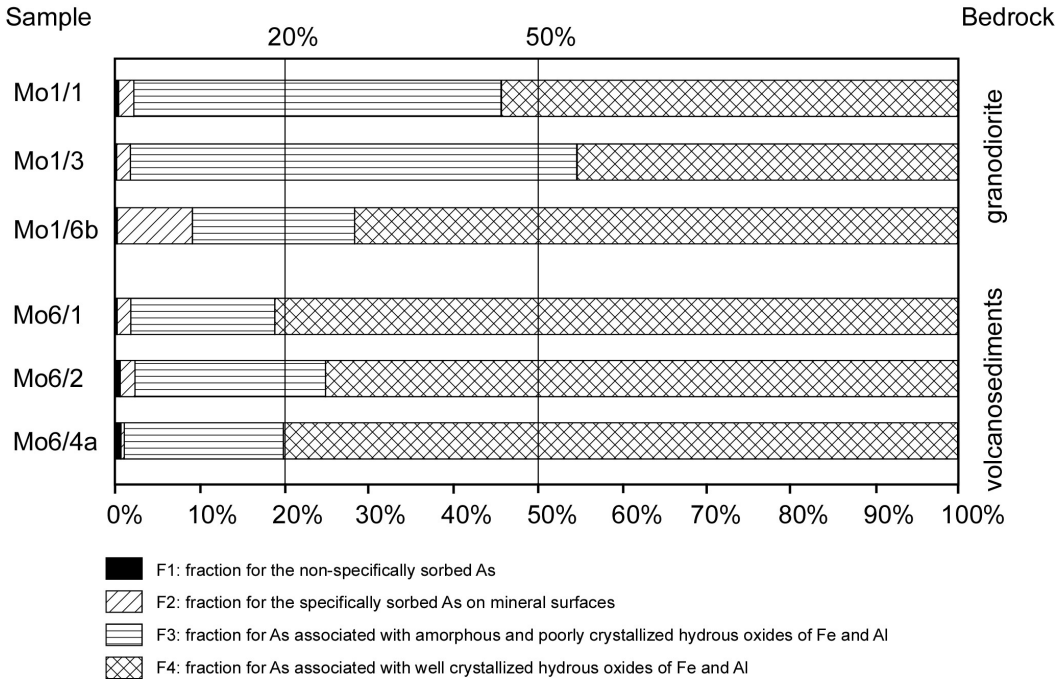

Fig. 12. Relative amounts of extracted As from particular fractions obtained by sequential extraction of the Mokrsko soil samples

5.5. Discussion

5.5.1. Representation and distribution of As-bearing minerals in soil profiles

In profile Mo1 arsenates were detected in all horizons, especially in the basal part. While in profile Mo2, the arsenates occur below the topsoil, in the middle section, and are absent in the base of the profile. Local enrichment by As secondary minerals at the base of the Mo1 profile is caused by the presence of broken, mineralised quartz vein in the decomposed bedrock. Distribution of arsenates in both profiles (Mo1 and Mo2) is a result of mechanical dissemination from decomposing mineralised quartz veins in outcrop during the soil evolution. The morphology of some arsenates (replacement or aggregation with rock-forming minerals) implies precipitation from As-rich solutions, as observed by Morin et al. (2000). We suggest that precipitation could proceed during the initial stage of the outcrop exposure, before the mature soil cover was developed. Contrary to well developed cubic crystals of pharmacosiderites described in the literature (e.g., Mutter et al., 1984; Peacor and Dunn, 1985; Walenta, 1994; Morin et al., 2002), our arsenates are clearly not a product of hydrothermal activity in the bedrock.

Making assumptions on the secondary mineral evolution and distribution in the soil above the volcanosedimentary bedrock is difficult because of the absence of a continuous and undisturbed soil profile to sufficient depth (the Cr horizon was not reached), as well as due to possible slope movements. The large number of structural types of FOHs indicates different physico-chemical parameters compared to soils above the granodiorite.

5.5.2. Selected soil properties versus secondary mineralisation: implication on stability of As-bearing minerals

The diversity of secondary As species is strongly influenced by type of primary ore mineralisation and the mobility of As depends on the soil type (cf., De Groot et al., 1998, De Brouwere et al., 2003; Tlustoš et al., 2004). Since the studied soil profiles are approximately similar in respect to their mineralogical and chemical compositions, and the primary ore in the bedrock is the same, variances in the pedological parameters are the main factor controlling the stability of the secondary minerals.

The difference in vegetation cover of the soil above the unforested granodiorite compared to the forested volcanosedimentary area plays an important role. It mirrors the contents of humus and values of pH in uppermost horizons which is notable regarding possible As binding in organic compounds (Turpeinen et al., 1999) and considering that the adsorption of As(V) onto goethite decreases with increasing pH (Goldberg, 1986; Raven et al., 1998). Increased exchangeable H^+ in samples in the lower part of the Mo1 profile is probably related to the continuing oxidation of arsenopyrite, which is preserved as relics in the mineralised geest. Together with the abundance of newly formed secondary minerals, this feature may also be reflected in the contents of other determined pedological parameters such as high concentration of exchangeable K^+, Na^+ and especially Ca^{2+} and Fe (Tamm). Increased exchangeable Ca^{2+} in the Mokrsko soils could possibly explain the low carbonate content and absence of calcite in the samples. Calcite was probably dissolved in the geest/soil environment, and together with weathered plagioclase, lead to Ca^{2+} cations being released

into solution (cf., Drahota and Pertold, 2005). The high content of Ca^{2+} and relatively high pH in soil above the granodiorite has a positive influence on the stability of Ca-Fe arsenates (Nishimura et al., 1985; Swash and Monhemius, 1996; Smith et al., 2002). Calcium and Ca-Fe arsenates originating from sulphide oxidation under surface or near sub-surface conditions have usually been described from those associations hosted by (or rich in) lime (Pieczka at al., 1998; Juillot et al., 1999; Frau and Ardau, 2004; Pactunc et al., 2004). However, results of this work indicate at a major significance of As trapping by Ca-Fe arsenates in soils developed from other types of bedrock.

Variability in composition and structure of FOHs in the soil profiles above the volcanosediments indicate a number of physico-chemical parameters changed in space and time (Mermut et al., 1985; Schwertmann and Taylor, 1989; Cornell and Schwertmann, 1996). It is likely that during soil evolution, other FOHs (cf., Fig. 5) were present, and these were then transformed to goethite (cf., Alpers et al., 1994; Bigham et al., 1996; Courtin-Nomade et al., 2005). In addition, amorphous and weakly crystallized ferrihydrite has been found in water saturated stream sediments and some soil samples in the Mokrsko area (Drahota and Pertold, 2005). This is important when considering the release of As into groundwaters, because the ageing of the amorphous and poorly crystallized iron (III) hydroxides may promote As desorption (Dzomback and Morel, 1990; Fuller et al., 1993). However, the goethites found in soils around Mokrsko have a high Fe/As ratio and are stable (Swash and Monhemius, 1994). This corresponds with the measurements of Drahota and Pertold (2005), which found very low concentrations of dissolved Fe (Mn, and Al) in streams of the Mokrsko catchment.

The abundance of FOHs in soils above the volcanosediments indicates relatively acidic environments over long-time scales (Foster et al., 1998; Pichler et al., 2001; Savage et al., 2000). This is also reflected in the common occurrence of jarosite, which mostly forms by pyrite oxidation under acidic conditions and is stable under relatively low pH (Strawn et al., 2002; Dold, 2003; Savage et al., 2004).

5.5.3. Succession model for mineralisation above the granodiorite bedrock

A working hypothesis based on the observations made above, and analytical determinations, has lead to the following simplified succession model, which agrees with published data. Unfortunately long-term agronomic exploitation (ploughing, fertilization, etc.) of the Mokrsko soils may partly depreciate the following interpretation.

First stage (corresponding with early oxidation in the mine wastes): Decomposition of sulphides causes low pH, crystallization of Fe arsenate as scorodite (cf., Dove and Rimstidt, 1985; Krause and Ettel, 1988; Bowell, 1994; Peters and Blum, 2003; Utsunomia et al., 2003; Filippi, 2004), the formation of metastable amorphous or weakly crystalline FOHs (Schwertmann and Taylor, 1989) and the precipitation of jarosite (e.g., Hudson-Edwards et al., 1999; Matera et al., 2003). Assuming the migration of As-rich solutions, crystallization of scorodite could occur around the primary source, as well as pseudomorphs of FOHs after cubic pyrite (cf., Cornell and Schwertmann, 1996; Foster et al., 1998; Savage et al., 2000; Pichler et al., 2001).

Second stage: Advanced soil development produces an increased availability of base cations, increases pH, disseminates arsenates into the soil profile, retards sulphide oxidation or consumption of most sulphides (Lumsdon et al., 2001). All these features probably evoked changes in arsenate

chemical composition and are represented by K-Ba (Ca) replacement (cf., Mutter et al., 1984; Morin et al., 2002), scorodite dissolution and related crystallization of As-containing FOHs (Dove and Rimstidt, 1985; Krause and Ettel, 1988; Juillot et al., 1999).

Third stage (present): Oxidation of the remaining exposed arsenopyrite proceeds under different conditions compared to the primary stage (higher pH, increased concentration of base cations, etc.). Under such conditions, crystallization of (or replacement by) other secondary minerals is expected, especially when the Fe arsenates precipitate at lower pH values than Ca arsenates (pH 1-2 vs. pH 3-4) (Robins and Glastras, 1987; and cf., Paktunc et al., 2004). Moreover, the continual re-crystallization of various FOHs onto the most stable goethites is likely (e.g., Alpers et al., 1994).

5.5.4. Data from sequential extraction versus mineralogical observations

Results from different sequential extractions developed to evaluate the As speciation in soils, are difficult to compare and reproduce as many different chemical reagents are used (cf., Gleyzes et al., 2002; Montperrus et al., 2002). In addition, some of the extraction steps used in sequential extractions are somewhat artificial. The so-called carbonate step (Ca-As fraction) is difficult to justify from a mineralogical point of view as Lombi et al. (2000) and Wenzel et al. (2001) found it doesn't contain As even in calcareous soils. Therefore it is more reliable to combine chemical and mineralogical methods.

Sample Mo1/6b has considerably higher content of As extracted from fraction F2 compared to other samples, which is a reflection that this sample does not represent a mature soil, but a decomposed geest with abundant unstable secondary As mineralisation. The As extracted from fractions F3 and F4 in all samples indicate As binding in surface complexes with more or less crystallized FOHs (Matera et al., 2003; Zhang et al., 2004). The highest amount of As extracted from fraction F4 is attributed to well crystallized FOHs, and are associated with samples from the profile Mo6, which corresponds well with the mineralogical composition (predominant goethite). Arsenic determined in fraction F3 of samples from profile Mo1 is higher than in samples from profile Mo6. This indicates easier extractability of As from arsenates than from FOHs. Absence of As in fraction F5 agrees with the mineralogical results and suggest complete decomposition of the primary sulphides during soil evolution (Lumsdon et al., 2001).

Despite a large range of As concentrations in the soil profiles (ca. 870-17,950 mg/kg of As), the relative portions (in %) are similar. This follows the consideration presented in Section 1, where we reason that As binding could be relatively strong in mature soils. If we liken sample Mo1/6b to a tailings material, where the secondary mineralisation is in progress, then it is not surprising that a notable proportion of the As (ca. 9 %) is relatively mobile compared to other samples tested.

However, we must take into account that the >0.125 mm fraction was studied by mineralogical methods, and the <2 mm fraction was leached by the sequential extraction. Matera et al. (2003) found that As was trapped in soils by amorphous FOHs in the fine soil fraction (<50 μm). Similar results confirming the significance of As association with Fe oxides or clay minerals in different size fractions have also been identified by Dudas (1987), Manful et al. (1994), and Kavanagh et al. (1997). This might explain why considerable amounts of As was extracted from fraction F3 in samples from the Mo1 profile, where FOHs were detected only rarely by mineralogical methods performed on substantially coarser mineral fraction.

5.6. Conclusion

Above the granodiorite bedrock the main As-carriers in two profiles from a flat agriculturally exploited area are pharmacosiderite, arseniosiderite, and to a lesser extent scorodite and goethite. Above the volcanosedimentary bedrock two profiles from a forested area have goethite, minor hematite and other indistinguishable FOHs, rare pharmacosiderite and also As-containing jarosite as the main As-carriers.

The different physico-chemical properties of the naturally contaminated soils studied, result in the heterogeneous nature of the As mineralogical speciation over a relatively small area, despite the secondary species being derived from one primary ore. From parameters determined in this study, we found the following to be significant for the diversification and stability of the As secondary minerals in the studied aerobic soils: presence of calcite in the bedrock and related content of exchangeable Ca^{2+} in soil, high content of oxalate Fe, and varying pH. The presence/absence of long-term vegetation cover influences the pedological parameters and thus plays an important role in forming and stability of the As minerals in soil.

Based on results of the sequential extraction, most of the As is bound relatively strongly to the soils (i.e. not easily available for plants) at the studied sites. In accordance with the mineralogical observations clear predominance of As associated to well crystallized FOHs was confirmed in soils above the volcanosediments. This also indicates the higher retention of As in these soils compared to soils with predominant arsenates (above the granodiorite bedrock), where a higher portion of As was extracted during the third extraction step (see Fig. 12). However, to evaluate selectivity of the sequential extraction employed in this work, more detailed studies combining the mineralogical and sequential leaching research on different size fractions is needed.

Acknowledgements

This research was supported by Institutional Research Plan no. AV0Z30130516 (Institute of Geology, AS CR, Prague) and by project no. 79-502 881 (EMOZMiD), financed by Rio Tinto Technology Development. The authors would like to express their thanks to V. Böhmová (Service Laboratory of Physical methods, Institute of Geology AS CR) and to J. Haloda (Laboratories of Geological Institute, Faculty of Sciences, Charles University, Prague) for assistance with the SEM/EMPA study. Pedological parameters were determined by H. Macurová (Research Institute of Ameliorations and Soil Conservation, Prague), the XRF analyses were performed by S. Randáková (Institute of Chemical Technology, Prague), the AAS analyses were performed by M. Burian and the ISP-OES measurement by J. Rohovec (both from Department of environmental geochemistry, Institute of Geology AS CR). The authors appreciate help and comments of Z. Pertold, A. Žigová and anonymous reviewers, which all helped to improve the manuscript. R.A. Lewis is acknowledged for improving the English.